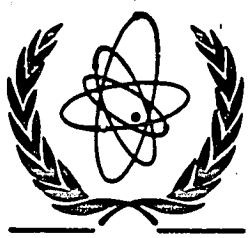

International Atomic Energy Agency

INDC(BLR)-002
Distr.: L

INDC INTERNATIONAL NUCLEAR DATA COMMITTEE

EVALUATION OF NEUTRON DATA FOR CURIUM-243

V.M. Maslov, E.Sh. Sukhovitskij, Yu.V. Porodzinskij,
A.B. Klepatskij and G.B. Morogovskij

Radiation Physics & Chemistry Problems Institute
220109 Minsk-Sosny, Belarus, CIS

December 1995

IAEA NUCLEAR DATA SECTION, WAGRAMERSTRASSE 5, A-1400 VIENNA

Reproduced by the IAEA in Austria
December 1995

INDC(BLR)-002
Distr.: L

EVALUATION OF NEUTRON DATA FOR CURIUM-243

Maslov V.M., Sukhovitskij E.Sh., Porodzinskij Yu.V., Klepatskij A.B., Morogovskij G.B.

Radiation Physics & Chemistry Problems Institute
220109, Minsk-Sosny, Belarus, CIS

Abstract

The evaluation of neutron data for ^{243}Cm is made in the energy region from 10^{-5} eV up to 20 MeV. The results of the evaluation are compiled in the ENDF/B-VI format .

This work is performed under the Project Agreement CIS-03-95 with the International Science and Technology Center (Moscow). The Financing Party for the Project is Japan. The evaluation was requested by Y. Kikuchi (JAERI).

1 Introduction

The advanced nuclear fuel cycle studies request the nuclear data of transplutonium isotopes[1]. The neutron data for curium isotopes are especially important in this respect. Recently we have evaluated the data for ^{242}Cm and ^{244}Cm nuclei, the data files[2,3] are stored in BROND library. In this work the evaluation of ^{243}Cm neutron data is performed. The next two isotopes, which neutron data would be evaluated within a next half a year, are ^{245}Cm and ^{246}Cm. The curium isotopes data to be evaluated were requested by the General Manager of Japan Nuclear data Center Dr. Y. Kikuchi. The quantities evaluated are resolved and unresolved resonance parameters, total, elastic and inelastic scattering, fission, capture, (n,2n) and (n,3n) reaction cross sections, angular and energy distributions of secondary neutrons, including partial (n,xn) and (n,xnf) reaction spectra, fission spectra and number of neutrons per fission. The incident neutron energy range covered is from 10^{-5} eV up to 20 MeV. The evaluated quantities are compared with JENDL-3 evaluation.

2 Resolved resonance region

2.1 Previous evaluations of resolved resonance parameters

The resonance parameter evaluation of ENDF/B-VI is based on total cross section data[4], measured from 0.01 eV up to 27 eV. Fission cross section[5] at thermal neutron energy was fitted with the negative resonance placed at E_r = -1.62 eV. In JENDL-3 evaluation the resonance parameters[6] up to 70 eV were adopted, however fission data[7] were not fitted. The purpose of current resonance parameter evaluation is to extend the resolved resonance region up to 100 eV and fit the total and fission data simultaneously.

2.2 Measured data fitting

2.2.1 Total cross section

There is only one measurement[6], encompassing the energy region 0.4÷66 eV, where the transmission was measured and total width and $2g\Gamma_n$ parameters are provided. We adopted these 52 resonance parameters.

2.2.2 Fission cross section

The bomb-shot fission cross section data[7] of Silbert are available in the energy region of 14 - 100 eV. Assuming realistic measurement conditions we

used fission data[7] and transmission data[6] to derive resonance parameters Γ_n^o, Γ_f, Γ_γ and E_r up to 100 eV.

2.3 Evaluated resonance parameters up to 100 eV

The whole resonance energy region is subdivided conditionally into three energy regions, according to the total and fission data availability and method of parameter derivation.

2.3.1 Energy region $10^{-5} \div 14$ eV

The JENDL-3 evaluated resonance parameters were adopted in this energy region, in fact, that is Anufriev et al.[6] parameters. The spin value of the resonances were assumed to be equal to the average value of the s-wave resonance spins, $J = 2.5$. Adopted parameters reproduce the data of Bemis et al.[8] and Mughabghab[9] on resonance integrals I_f and I_γ and thermal fission and capture cross sections.

2.3.2 Energy region $14 \div 63$ eV

The resonance parameters Γ, $2g\Gamma_n$ and E_r are derived by simultaneous analysis of Silbert[7] data on fission cross section and transmission data[6] . Assuming realistic measurement conditions, the total cross section data are constructed on the basis of available resonance parameters[6]. Both data sets are used to get a self-consistent set of resonance parameters: Γ_n^o, Γ_f, Γ_γ and E_r. Two assumptions are adopted: 1) the statistical weight of fission data is two times lower than that of total cross section data; 2) the radiative width Γ_γ is allowed to fluctuate between 20 and 70 meV. Figures 2.1, 2.3, 2.5 and 2.7 show the comparison of total cross sections, calculated with present and JENDL-3 evaluated parameters. The discrepancies in total cross section are correlated with the differences in Silbert fission data[7] fitting (see figs. 2.2, 2.4, 2.6 and 2.8).

2.3.3 Energy region $63 \div 100$ eV

There are data on total and neutron resonance width of Anufriev et al.[6] , based on which we construct total cross section data. The fission data[7] are available as well. There is a resonance around 66 eV with anomalous $2g\Gamma_n$ and Γ values. The fission data[7] show 6 resonances grouped around 66 eV, their $2\Gamma_n$ and Γ values being essentially smaller (see fig. 2.8). The appropriate resonances in total cross section are shown on fig. 2.7. Above 66 eV 47 more resonances were distinguished in fission cross section data. The data fit is shown on fig. 2.9.

2.3.4 Resonance parameter analysis

The average resonance parameters, thermal cross sections and resonance integrals of current and JENDL-3 evaluations are compared in Table 2.1.

Table 2.1

	ENDF/B-VI	JENDL-3	This evaluation
$<\Gamma_n^0>$, meV	0.6595	0.3282 – – – – 0.2612[1)]	0.2405 – – – – 0.2581[1)]
$<\Gamma_\gamma>$, meV	40.0	40.0	40.23 – – – – 39.46[1)]
$<\Gamma_f>$, meV	370.688	322.264 – – – – 304.6731)	334.821 – – – – 284.501[1)]
σ_t , barn	755.791	757.514	752.419
σ_γ , barn	57.9990	130.160	130.523
σ_f , barn	691.134	617.427	613.319
σ_n , barn	6.65766	9.92651	8.57665
g_γ	1.00805	0.98543	0.98549
g_f	1.00896	1.00771	1.00773
I_γ , barn	248.044	198.217	211.665
I_f , barn	1942.43	1552.84	1530.98

[1)] up to 63 eV.

The thermal total σ_t,capture σ_γ,and scattering σ_n cross sections, $g_\gamma-$, and g_f-factors, as well as resonance integrals $I\gamma$ and I_f values are calculated with a code INTER[10].

The difference in thermal scattering cross section σ_n is due to scattering radius value of 9.4757 fermi, which is taken from the coupled channel calculations (10 fermi was assumed in JENDL-3). Up to 63 eV incident neutron energy the total and fission cross sections, calculated with current and JENDL-3 parameters are rather compatible. The differences around 66 eV are due to resolving of multiplet around 66 eV using fission data[7]. This 66.03 eV resonance, if not resolved, would appreciably change the average values of $<\Gamma_n^o>$ and $<\Gamma_f>$ (see Table 2.1).

To parameterize the fission data in energy region of 63-100 eV 53 resonances are involved. The values of $<\Gamma_n^o> = 0.17$ meV and $<D_{obs}> =$ 0.71 eV are compatible with appropriate values for the energy region of 0-70 eV, derived with missing of levels taken into account (see below).

3 Unresolved resonance region

3.1 Review

Unresolved resonance region of ^{243}Cm is supposed to be from 0.1 keV up to 42.1743 keV. The lower energy is the end-point of resolved resonance region, the upper energy is the threshold energy of the inelastic scattering. We supposed $s-$, $p-$ and $d-$wave neutron-nucleus interactions to be effective. We suppose also the (n,γf) reaction to be important here due to high fissility of ^{244}Cm compound nucleus.

3.2 The s-wave average resonance parameter evaluation

3.2.1 Estimate of resonance level missing influence on $< D_{obs} >$ and $< S_0 >$

The preliminary estimates of average partial widths were obtained by averaging the evaluated resolved resonance parameters. They are as follows

$< g\Gamma_n^o >= 2.405 \times 10^{-4}$ (eV)$^{1/2}$
$< \Gamma_f > = 0.335$ eV
$< D_{obs} > = 0.964$ eV
$< \Gamma\gamma > = 0.0402$ eV

Note that due to missing of weak resonances these values overestimate actual reduced neutron width $< g\Gamma_n^o >$ and neutron resonance spacing $< D_{obs} >$. To get a physically justified values for $< g\Gamma_n^0 >$ and $< D_{obs} >$ we employ a method , which is described elsewhere[11]. Both reduced neutron width and neutron resonance spacing distributions are obtained in a unified approach. We take into account the correlation of weak resonance missing and resonance missing due to poor experimental resolution simultaneously. The resolution function parameters as well as $< g\Gamma_n^o >$ and $< D_{obs} >$ are obtained by maximum likelyhood method when comparing experimental distributions of reduced neutron width and resonance spacing with Porter-Thomas and Wigner distributions, modified for the resonance missing.

3.2.2 Evaluation of $< D_{obs} >$, $< S_0 >$, $< \Gamma_\gamma >$ and $< \Gamma_f >$ based on the resonance parameters

To evaluate average neutron resonance spacing $< D_{obs} >$ and neutron strength function S_0 we employ our method[11] to the resolved resonance data base. We suppose that only data up to 70 eV should be taken into account, since at higher energies neutron resonance widths were deduced from bomb-shot data[7] on fission cross section. The final evaluated values are:

$< S_0 >= 1.458 \times 10^{-4}$ (eV)$^{-1/2}$

$< D_{obs} > = 0.679$ eV

Average fission and radiation widths are virtually insensitive to resonance missing, so we used values obtained by averaging of resolved resonance parameters up to 100 eV.

Figure 3.1 shows the comparison of theoretical reduced neutron width distributions and experimental one. Figure 3.2 shows the same comparison for neutron resonance spacing. Both figures are obtained for energy interval 0-35 eV. Figures 3.3 and 3.4 show the same comparisons for energy intervals of 0-35 eV and 0-70 eV. Theoretical distributions show the effect of resonance missing on width and spacing distributions. The theoretical distributions which were fitted to the experimental distribution within the maximum likelihood method by varying the resolution parameters is called an expected distribution. The figures 3.1-3.4 show that the expected distributions are consistent with the experimental ones for both energy intervals. That is why the $< D_{obs} >$ and S_0 estimates could be considered reliable.

3.3 The p- and d-wave average resonance parameter evaluation

3.3.1 Neutron width

Average neutron width is calculated as follows

$$< \Gamma_n^{lJ} > = S_l < D_J > E^{1/2} P_l,$$

where P_l is the transmission factor for the lth partial wave, which was calculated within black nucleus model. The p-wave neutron strength function $S_1 = 2.12 \times 10^{-4}$ $(\mathrm{eV})^{-1/2}$ was calculated with the optical model, using the deformed optical potential, described below. The d-wave neutron strength function $S_2 = 1.458 \times 10^{-4}$ $(\mathrm{eV})^{-1/2}$ is supposed to be equal to the S_0 value. Since the d-wave contribution is rather small, the impact of this approximation is negligible.

3.3.2 Neutron resonance spacing

Neutron resonance spacing $< D_J >$ was calculated with the phenomenological model[12], which takes into account the shell, pairing and collective effects. The the main parameter of the model $\tilde{a}$ was normalized to the observed neutron resonance spacing $< D_{obs} > = 0.679$ eV.

3.3.3 Fission width

Fission widths are calculated within a double-humped fission barrier. Energy and angular momentum dependence of fission width is defined by the transition state spectra at inner and outer barrier humps. We constructed

both spectra by supposing the triaxiality of inner saddle and mass asymmetry at outer saddle. We will describe them below. The calculated widths $< \Gamma_f^{2+} >$ and $< \Gamma_f^{3+} >$ are normalized to the adopted average fission width $< \Gamma_f >= 0.355$ eV.

3.3.4 Radiative capture width, role of (n,γf) reaction

Energy and angular momentum dependence of radiative capture width are calculated within a two-cascade γ-emission model with allowance for the (n,γf) reaction competition to the (n,$\gamma\gamma$) reaction. The (n,$\gamma\gamma$) reaction is supposed to be a radiative capture reaction. The radiative capture width was normalized to the $< \Gamma_\gamma > = 40.2$ meV. (For details see Ghapter IV).

3.4 Cross section evaluation in the region 0.1-42 keV

3.4.1 Fitting of fission cross section structure

There are only bomb-shot fission data of Silbert[7] available in the unresolved resonance region. The adopted average resonance parameters describe these data rather well (see fig.3.5). To fit the data at chosen energy intervals we varied the neutron strength function S_0 value. The possibility of varying $< \Gamma_f^{2+} >$ or(and) $< \Gamma_f^{3+} >$ was rejected, since inherently the fission width should fluctuate less vigorously, than neutron width because of greater degrees of freedom number. That decision was justified by the experience obtained in case of ^{235}U and ^{239}Pu neutron data evaluation. For these nuclei there are measured data on total and fission cross sections. Varying s-wave strength function S_0 values to fit total cross section data in chosen intervals we can reproduce simultaneously most of the fission cross section fluctuations. The S_0 values for chosen neutron energy intervals are given in Table 3.1.

3.4.2 Drawbacks of ENDF/B-VI format and associated inconsistencies in neutron cross sections

Within ENDF/B-VI format we can not distinguish between (l, J, j) reaction channels with different channel spin values $j = l \pm 1/2$. Specifically, channels $(l = 1, J = 3, j = 1/2)$ and $(l = 1, J = 3, j = 3/2)$ are treated as a lumped channel $(l = 1, J = 3)$ with neutron degrees of freedom ν=2, then the average neutron width $< \Gamma_n^{lJ} >$ for $(l = 1, J = 3)$ channel equals

$$< \Gamma_n^{13} >= 2 S_1 P_1 \sqrt{E} D_3$$

This results in an increase of elastic scattering cross section as compared with a case when one treats channels $(l = 1, J = 3, j = 1/2)$ and $(l = 1, J = 3, j = 3/2)$ separately. Within ENDF/B-VI format constraints the elastic

Table 3.1

Average cross sections in unresolved resonance region for ^{243}Cm

E, keV	$S_0 \times 10^{-4}$,(eV)$^{-0.5}$	σ_f , b	σ_γ , b	σ_γ , b(JENDL-3)
0.10	1.596	51.07	12.90	8.77
0.12	1.259	36.90	9.36	7.67
0.17	0.901	22.30	5.67	5.65
0.25	1.172	23.72	5.97	4.71
0.35	0.990	16.99	4.28	3.66
0.45	1.056	15.92	3.99	3.27
0.55	1.152	15.64	3.90	3.17
0.70	1.319	15.74	3.88	3.01
0.90	1.386	14.51	3.55	2.74
1.20	1.325	12.02	2.93	2.37
1.70	1.437	10.86	2.62	1.92
2.50	1.449	9.01	2.15	1.56
3.50	1.393	7.37	1.75	1.28
4.50	1.297	6.16	1.46	1.13
5.50	1.348	5.80	1.36	1.02
7.00	1.394	5.35	1.24	0.90
9.00	1.442	4.92	1.13	0.79
12.00	1.500	4.50	1.02	0.71
17.00	1.550	4.03	0.91	0.60
25.00	1.500	3.47	0.78	0.52
35.00	1.432	3.09	0.69	0.45
42.1743	1.362	2.95	0.62	0.43

enchancement would be too strong because of artificial duplication of elastic scattering neutron width. Moreover, the increase of neutron number of degrees of freedom decreases the competition of fission reaction channel. Henceforth the fission and capture reactions, calculated with standard ENDF/B utility codes are decreased as compared with the results of physically correct approach . The magnitude of this discrepancy at 42 keV incident neutron energy amounts to $\sim 3\%$ in fission cross section.

3.4.3 Comparison of current and JENDL-3 evaluated data

Evaluated fission cross sections of this work and JENDL-3 are not showing any discrepancies, since both evaluations are based on Silbert data[7]. The discrepancies are noticed when comparing the (n, γ) reaction cross sections

(see fig. 3.6) Current evaluated cross section is almost 1.5 times as large as JENDL-3 evaluated capture cross section. This discrepancy is due to strong $(l, J)-$ channel dependence of fission width in our approach. This dependence is due to adopted transition states spectra structures (see below). Specifically the ratio of $<\Gamma_f^{2+}>/<\Gamma_f^{3+}> = 2.5$ is almost independent on incident neutron energy, that will lead to the increased capture reaction cross section for the $(l = 0, J = 3)$ channel as compared with JENDL-3 approach. In JENDL-3 approach the fission width value is channel, i.e. spin and parity independent, while its value of 1.481 eV is anomalously high. With this high fission width Silbert' data[7] can not be reproduced in our approach.

4 Fast neutron cross sections

The measured data on fission cross section[13] show an unreasonable structure in the energy range 0.1÷1 MeV. They are also rather discrepant with previous data[14]. So, the available fission data fit can not be used as constraint for (n, n') and (n, γ) reaction cross section evaluation. We reproduce the average fission widths within double-humped fission barrier model. To fix fission channel parameters the systematic trends, noticed in measured fission data[15] on ^{245}Cm(n,f) and ^{247}Cm(n,f) are also used.

4.1 Optical potential

The deformed optical potential for n+^{243}Cm interaction is chosen in the following way. The starting values for the potential parameters were those for n+^{238}U interaction[16]. The isotopic dependences of real and imaginary parts of the potential were calculated using the optical potential parameter systematics[17]. Six levels of the ground state band ($5/2^+$,$7/2^+$,$9/2^+$, $11/2^+$,$13/2^+$, $15/2^+$) are coupled, since the sixth level is missing in compilation[18], it was added as $E_J = A(J(J+1) - K(K+1))$. The deformation parameters β_2 and β_4 are obtained by fitting S_0 value of 1.458×10^{-4} $(\mathrm{eV})^{-1/2}$. The original geometry parameters[16] are modified to fit measured data for N-odd targets above 10 MeV. This procedure of parameter fitting is well tested in case of ^{239}Pu, ^{235}U and ^{233}U targets. The potential parameters are as follows:

$$V_R = 46.49 - 0.3E, MeV, r_R = 1.26 fermi, a_R = 0.615 fermi$$

$$W_D = \begin{cases} 3.77 + 0.4E, MeV, & E < 10MeV, r_D = 1.24 fermi, a_D = 0.5 fermi \\ 7.77 MeV, & E > 10MeV \end{cases}$$

$$V_{SO} = 6.4MeV, r_{SO} = 1.120 fermi, a_{SO} = 0.470 fermi, \beta_2 = 0.233, \beta_4 = 0.067$$

The s- and p-wave strength functions and potential scattering cross sections, calculated with this potential parameters in a coupled channel approach at incident neutron energy of 70 $eV$are:

$S_0 = 1.43 \times 10^{-4}(\mathrm{eV})^{-1/2}$ $S_1 = 2.12 \times 10^{-4}(\mathrm{eV})^{-1/2}$ $R_p = 9.4757 fermi$

The reaction cross sections, calculated with deformed optical potential and spherical optical potential, which is used in JENDL-3 evaluation, are compared on fig.4.1. The significant differences below 1 MeV and above 10 MeV would manifest in inelastic scattering cross sections and $(n, 3n)$ cross section. The total cross sections are also rather different (see fig.4.2), while elastic scattering cross section appear to be rather close (see fig. 4.3).

4.2 Fission cross section

The bomb-shot data of Fomushkin et al.[14,13] published in 1987 and 1990, respectively, appear to be rather different from each other. The latter data are consistently higher than the former in the energy region from 0.1 MeV up to 1 MeV. Above 1 MeV incident neutron energy they argue more steep decrease of fission cross section with energy. Both data sets are incompatible with Silbert[7] data around 40 keV, which were fitted in unresolved resonance region. Data of Silbert[7] are well described with average resonance parameters up to 42 keV (see fig. 3.5). The data of Fomushkin et al.[14] appear unrealistically high in the energy region from 0.1 MeV up to 1 MeV. The bomb-shot data of Fullwood et al.[19] and Silbert[7] are consistently higher than both data sets of Fomushkin et al. above 100 keV (see fig. 4.4). So we consider the data base inconsistent to fit any particular data set. We proceed as follows. The fission cross section is calculated with the statistical model, the fission widths for $s-$wave neutrons Γ_f^{2+} and Γ_f^{3+} are fitted at 0.1 keV by varying transition spectra band-heads to get average fission width of 0.355 eV. The fission cross section above 1 MeV incident neutron energy was adopted to be consistent with data of Fomushkin et al.[13,14] The slope of the cross section with energy in the first plateau region is consistent with the systematic trends[20]. It is less steep than that of Fursov et al.[15] data for ^{245}Cm(n,f) and ^{247}Cm(n,f). The comparison of calculated cross section with JENDL-3 evaluation and data of Fomushkin et al.[13,14] is shown in fig. 4.5.

4.2.1 Fission transmission coefficient and transition state spectrum

The discrete transition spectra contribution to the fission transmission coefficient is dependent upon the inner and outer saddle order of symmetry for ^{244}Cm fissioning nucleus. Due to the axial asymmetry at the inner saddle[21] the respective 2^+-band-heads are lowered as compared with the respective positions of 2^+ -band-heads at ground state deformation. The positions of negative parity bands $K^\pi = 0^-, 1^-, 2^-$ at outer saddle are lowered due to

mass asymmetry[21]. With transition state spectra thus defined (see Table 4.1) the fission barrier parameters are obtained (see table 4.2). The average fission width $< \Gamma_f^{2+} > = 0.52$ eV, $< \Gamma_f^{3+} > = 0.22$ eV are calculated. The adopted transition state spectrum leads to rather strong spin and parity dependence of fission width $< \Gamma_f^{J\pi} >$.The cut-off energy of discrete transition state spectra is assumed 1.0 MeV, at higher excitation energy axially symmetric fissioning nucleus level density $\rho(U) = T_f^{-1} \exp((U - U_o)/T_f)$ is calculated in constant temperature approximation. The respective parameters T_f and U_o are defined at the matching point $U_c = 4.6MeV$ of the continuum part of the transition state spectrum represented with the phenomenological model[12], which takes into account pairing, shell and collective effects at saddle deformations. After that the effects of non-axiality and mass asymmetry are included. The detailed procedure of calculating fission trasmission coefficient is described elsewhere[22]. The respective parameters: shell correction at saddles δW, correlation function Δ, quadrupole deformation ε,and momentum of inertia at zero temperature $F_0/\hbar^2$ are given in Table 4.3. The effect of two-quasi-particle states on level density of even-even ^{244}Cm fissioning nucleus is also modelled[22]. It defines the fission cross section shape at incident neutron energies $\sim 0.4 \div 2$MeV.

Table 4.1

Transition spectra band-heads of ^{244}Cm

inner saddle		outer saddle	
K^π	E_{K^π}, MeV	K^π	E_{K^π}, MeV
0^+	0.0	0^+	0.0
2^+	0.1	2^+	0.3
0^-	0.4	0^-	0.0
1^-	0.4	1^-	0.1
2^+	0.3	2^+	0.3
2^-	0.4	2^-	0.1
0^+	0.8	0^+	0.8
0^+	0.8	0^+	0.8

Table 4.2

Fission barrier parameters of ^{244}Cm

Barrier	Barrier height, MeV	Curvature, MeV
inner	6.43	0.9
outer	5.10	0.6

Table 4.3
Level density parameters of ^{244}Cm fissioning nucleus and residual nucleus ^{243}Cm

Parameter	inner saddle	outer saddle	neutron channel
δW, MeV	2.5	0.6	-2.692
$\triangle$, MeV	$\triangle_0$ +0.05	$\triangle_0$ +0.05	$\triangle_0$
ε	0.6	0.8	0.24
$F_0/\hbar^2$, MeV^{-1}	100	200	73

Below incident neutron energy 0.4 MeV the neutron cross sections are calculated within Hauser-Feshbach approach with a width fluctuation correction taken into account. For width fluctuation correction calculation only Porter-Thomas fluctuations are taken into account. Effective number of degrees of freedom for fission channel is defined at the higher (inner) saddle as $\nu_f^{J\pi} = T_f^{J\pi}/T_{f\,max}^{J\pi}$, where $T_{f\,max}^{J\pi}$ is the maximum value of the fission transmission coefficient $T_f^{J\pi}$. Above incident neutron energy of 0.4 MeV the Tepel et al.[23] approach is employed. The calculated fission cross section is compared with experimental data on fig. 4.5. The comparison with JENDL-3 evaluated fission cross section is shown on figure 4.5.

4.2.2 Fission cross section above emissive fission threshold

The first chance fission cross section of ^{244}Cm nucleus above the emissive fission threshold is fixed with the level density and fission barrier parameters[22] (see Tables 4.2, 4.3) and secondary neutron spectra parameterization. A consistent description of a complete set of measured data on (n,f), (n,2n) and (n,3n) for ^{238}U and ^{235}U targets was accomplished with the secondary neutron spectra parameterization[24], which is used here. The ^{243}Cm fission barrier parameters are fixed in ^{242}Cm(n,f) data analysis. The other fissioning nuclei ^{242}Cm and ^{241}Cm fission barrier heights are obtained from Howard and Moller shell correction method calculations[21] and systematics parameter trends.

The calculated fission cross section is drastically different from JENDL-3 evaluated curve above (n,nf) reaction threshold (see fig. 4.6). The reason of discrepancy is the extremely low contribution of (n,nf) reaction and, on the other hand, extremely high contribution of (n,2nf) reaction to the total fission reaction cross section in JENDL-3 evaluation. The measured data of Fomushkin et al.[25] appear to be higher than reaction cross section at 14.8 MeV, so they are incompatible with our evaluation.

4.3 Inelastic scattering cross section

The inelastic scattering cross section is calculated with the statistical codes STAT and STAPRE[26]. The discrete level excitation (compound and direct), continuum excitation and pre-equilibrium emission contribute to the inelastic scattering cross section. The low-lying level scheme of Nuclear Data Sheets[18] appear incomplete at excitation energy as low as 0.2 MeV. The first levels, which were added are the K^{π} =$1/2^{+}$ band levels J = 5/2 ,7/2, 11/2,13/2 (J = 1/2, 3/2 and 9/2 levels are present).The ground state band levels J=15/2 and J=17/2 were also added. Then the negative parity K^{π}= $5/2^{-}$ band and the positive parity band K^{π} = $3/2^{+}$ were added according to systematics for ^{235}U and ^{239}Pu nuclei. The number of excited levels in ^{243}Cm is 24 up to 0.4 MeV (see Table 4.4), while in JENDL-3 evaluation there are only 13 levels up to 0.769 MeV. The continuum level density below excitation energy U_c = 3.8 MeV is calculated with the constant temperature model (Fig. 4.7)

$$\rho(U) = T_0^{-1} \exp((U - U_o)/T_0),$$

here the constant temperature model parameters are: energy shift U_0 = -1.1243 MeV, nuclear temperature T_0 = 0.4069 MeV. At higher excitation energies the phenomenological model[12] is used. The main model parameter $\tilde{a}$ for ^{243}Cm residual nucleus is obtained by fitting the evaluated neutron resonance spacing[2] of ^{243}Cm compound nucleus $< D_{obs} >$= 8 eV.

4.3.1 Compound inelastic scattering

The residual nucleus ^{243}Cm level density modelling changes drastically the inelastic scattering cross section below 5 MeV as compared with JENDL-3 evaluation (see fig. 4.8). Below 1 MeV incident neutron energy only small part of the discrepancy is due to direct inelastic scattering of the ground state band levels. Below 0.4 MeV incident neutron energy the discrepancy is due to strong inelastic scattering for the K^{π}= $1/2^{+}$ band levels, which produces a dip in fission cross section around 0.4 MeV (see fig.4.4 and 4.5). Above 1 MeV incident neutron energy inelastic scattering to the continuum

gives a major contribution to the total inelastic scattering cross section. Above 5 MeV incident neutron energy pre-equilibrium emission and direct inelastic scattering are the two reaction mechanisms which define inelastic scattering cross section (see fig. 4.8). The pre-equilibrium model parameters were tested by model description of ^{238}U+n interaction secondary neutron spectra and consistent description of fission and (n,xn) reaction data for major actinides[24].

Table 4.4

Level scheme of ^{243}Cm

$E_{J\pi}$, MeV	J	π	K	band	
0.000	5/2	+	5/2	A	
0.042	7/2	+	5/2	A	
0.0874	1/2	+	1/2	B	
0.0939	9/2	+	5/2	A	
0.094	3/2	+	1/2	B	
0.133	7/2	+	7/2	C	
0.140	5/2	+	1/2	B	*
0.153	11/2	+	5/2	A	
0.158	7/2	+	1/2	B	*
0.164	9/2	+	7/2	C	
0.219	13/2	+	5/2	A	
0.228	11/2	+	7/2	C	
0.260	9/2	+	1/2	B	
0.280	11/2	+	1/2	B	*
0.300	15/2	+	5/2	A	*
0.305	5/2	-	5/2	E	*
0.310	3/2	+	3/2	D	*
0.311	13/2	+	7/2	C	*
0.320	7/2	-	5/2	E	*
0.340	5/2	+	3/2	D	*
0.354	9/2	-	5/2	E	*
0.380	13/2	+	1/2	B	*
0.390	15/2	+	7/2	C	*
0.395	11/2	-	5/2	E	*
0.400	17/2	+	5/2	A	*

*) added

4.3.2 Direct inelastic scattering

The direct inelastic scattering changes the shape of ground band levels excitation cross sections above 1 MeV incident neutron energy (see Figs. 4.9 - 4.13). The calculations were accomplished with the code COUPLE. This mechanism defines partly the hard-energy tail in total inelastic scattering cross section (see fig. 4.8).

4.4 Radiative capture cross section

The radiative capture cross section is calculated within a statistical approach up to 5 MeV. Radiative capture strength function $S_{\gamma 0} = 592.05$. At higher incident neutron energies we assume radiative capture cross section to be 1mbarn. The radiative capture width was calculated with (n,γf) and (n,γn') reactions competition against "true" capture reaction (n,$\gamma\gamma$). The role of (n,γf) and (n,γn') reactions is illustrated on fig. 4.14 by sharp decrease of capture cross section above 0.5 MeV incident neutron energy, as compared with JENDL-3 evaluation.

4.5 Cross sections of (n,2n) and (n,3n) reactions

The current and JENDL-3 evaluated (n,2n) and (n,3n) cross sections are drastically different. The magnitude of (n,2n) cross section below the (n,2nf) reaction threshold is defined by (n,nf) and (n,2n) rection competition. The reaction cross sections of this work and JENDL-3 below the (n,2nf) reaction threshold virtually coinside (see fig. 4.1). The difference between (n,2n) reaction cross sections of present and JENDL-3 evaluations is due to unrealistically low contribution of (n,nf) reaction to the total fission cross section in JENDL-3 evaluation and steep decrease of (n,nγ) reaction cross section of JENDL above 5 MeV (see fig. 4.15). In case of (n,3n) reaction the difference in reaction cross section above 11 MeV (see fig. 4.1) contributes essentially to the discrepancy, shown on fig. 4.16.

5 Energy distributions of secondary neutron spectra

There is no measured data on secondary neutron spectra except average fission neutron spectrum energies. To calculate neutron energy distributions of (n,xnγ) and (n,xnf), x=1, 2, 3, reactions a simple Weisscopf-Ewing evaporation model[27] is used, with which the partial spectra are obtained. The pre-equilibrium emission of first neutron is included.

5.1 Model calculations of (n,nx) reaction spectra

The first neutron spectra for the reaction (n,nx) is the sum of evaporated and pre-equilibrium emitted neutron contributions. The pre-equilibrium emission contribution is calculated with parameter systematics tested in case of n+^{238}U and n+^{235}U interactions[24,27]. Figure 5.1 shows the spectra of 1st neutron of the reaction (n,nx) and its partial contributions of (n,nγ), (n,2n), (n,nf) (n,2nf) and (n,3n) reactions. Figure 5.2 shows the spectra of 2nd neutron of the reaction (n,2nx) and its partial contributions of (n,2nγ), (n,3n) and (n,2nf) reactions. Figure 5.3 shows the spectra of 3d neutron of the reaction (n,3nx). The neutron spectra shown on figs. 5.1-5.3 are normalized to unity.The incident neutron energy is 14 MeV. The inclusion of pre-equilibrium emission changes significantly the average energies of emitted neutron spectra. The most significant is the change of first neutron spectra of (n,nγ) reaction. That is shown in Table 5.1, where the average secondary neutron energies for current and JENDL-3 evaluations are compared.

Table 5.1 Average energies of secondary neutron spectra

E_n, MeV	1st neutron average energy, MeV									
	n, n'		n, 2n		n, n'f		n, 3n		n, 2n'f	
	pres.	J - 3	pres.	J - 3	pres.	J-3	pres.	J - 3	pres.	J-3
2.0	0.52	0.70								
7.0	2.57	1.03	0.81	1.03	0.45					
14.0	9.95	1.48	3.98	1.48	2.71		0.49	1.48	1.02	
20.0	16.0	1.78	10.4	1.78	4.42		2.64	1.78	3.10	

E_n, MeV	2nd neutron average energy, MeV						3d neutron	
	n, 2n		n, 3n		n, 2nf			
	pres.	J - 3	pres.	J - 3	pres.	J-3	pres.	J - 3
7.0	0.20	0.71						
14.0	0.87	0.99	0.44	1.05	0.75		0.15	0.72
20.0	0.82	1.38	1.19	1.39	1.19		0.66	0.79

The 1st neutron spectra of (n,nf) reaction also becomes harder and that influences on the prompt fission neutron spectra. On the other hand, the spectra of 2nd and 3d neutrons become softer.

5.2 Prompt fission neutron spectra

Prompt fission neutron spectra were calculated within the framework of Madland-Nix model[28].

5.2.1 Model calculations of prompt fission neutron spectra

The model parameters, which should be defined are the following.

5.2.1.1 Fragment masses. The fragment masses are defined as $A_L = 104$ and $A_H = 140$, in accordance with fission product yields[29]. Fragment charges are defined as even values, closest to the ratios of

$<A_{L,H}> / (Z_{L,H} \mp 0.5) = A_F/Z_F$.

The average fragments adopted are ^{104}Mo and ^{140}Xe.

5.2.1.2 Energy parameters. Average total fission energies $<E_R>$ and neutron binding energies are taken from Wapstra et al.[30] Total fragment kinetic energies is calculated with Viola et al.[31] systematics:

$<TKE> = (0.1189 \pm 0.0011)\ Z^2/A^{1/3} + (7.3 \pm 1.5)$ MeV.

The resulted values of <TKE> are then varied to fit ν_p at thermal energy.

5.2.1.3 Other parameters. The level density parameter of the fermi-gas model is calculated as $a = A_F/10.2$, MeV^{-1}. Becchetti-Greenlees[32] spherical optical potential parameters are employed to calculate compound cross section.

5.2.2 Prompt fission neutron spectra evaluation

Below emissive fission threshold prompt fission neutron spectra are calculated with the parameters given for ^{244}Cm in Table 5.2.

Table 5.2

Parameters of the Madland-Nix model

Fissioning nucleus	Average light fragment	Average heavy fragment	$< E_R >$, MeV	$< TKE >$, MeV	B_n, MeV
^{244}Cm	^{104}Mo	^{140}Xe	209.722	185.800	6.799
^{243}Cm	^{103}Mo	^{140}Xe	210.119	186.024	5.694
^{242}Cm	^{102}Mo	^{140}Xe	209.245	185.420	6.971

Figures 5.4, 5.5 show the comparison of calculated prompt fission neutron spectra with maxwellian spectra (T = 1.408 MeV) of JENDL-3. Average energy of fission spectrum is 2.213 MeV, it is compatible with measured datum of 2.15±0.06 MeV of Zhuravlev et al[33].

Above emissive fission threshold the fission neutron spectra $N(E)$ is the superposition of emissive fission spectra, i.e.

$$N(E) = (\frac{\sigma_{nf}}{\sigma_{nF}}\nu_1 N_1(E) + \frac{\sigma_{nn'f}}{\sigma_{nF}}[\Phi_{nn'f}(E) + \nu_2 N_2(E)]$$
$$+\frac{\sigma_{n2nf}}{\sigma_{nF}}\left[\Phi^1_{n2nf}(E) + \Phi^2_{n2nf}(E) + \nu_3 N_3(E)\right])/$$
$$\left[\frac{\sigma_{nf}}{\sigma_{nF}}\nu_1 + \frac{\sigma_{nn'f}}{\sigma_{nF}}(1+\nu_2) + \frac{\sigma_{n2nf}}{\sigma_{nF}}(2+\nu_3)\right],$$

where σ_{nF}, σ_{nf}, $\sigma_{nn'f}$, σ_{n2nf} are the total and i-th chance fission cross sections (i = 1,2,3); $\Phi_{nn'f}$, Φ^1_{n2nf}, and Φ^2_{n2nf} are emitted neutron spectra: for (n,nf) reaction, 1st and 2nd neutrons of (n,2nf) reaction, respectively; ν_i and N_i are multiplicity and prompt neutron spectra for the i-th fissioning nucleus. The pre-equilibrium emission of the first neutron is included, the $\Phi^i_{n,xnf}$ spectra for the emissive fission are calculated with the model, described in 5.1. This influences the prompt fission neutron multiplicity ν_i and prompt neutron spectra N_i as well as N(E) and ν(E), that is illustrated in Table 5.3 for two incident neutron energies, $<E_i>$ denotes average prompt fission netron energy of i-th fissioning nucleus, <E> is the average fission neutron energy, $<E_{n'f}>$, $< E_{2nf} >^1$ and $< E_{2nf} >^2$are the average anergies of neutrons, emitted in (n,nf) and 1st and 2nd neutrons emitted in (n,2nf) reactions, respectively.

Table 5.3

	E_n = 7 MeV		E_n = 14 MeV	
Quantity	M-N model[28]	This work	M-N model[28]	This work
$< E_1 >$	2.368	2.368	2.508	2.508
ν_1	4.341	4.341	5.224	5.224
$< E_{n'f} >$	1.145	0.446	1.607	2.705
$< E_2 >$	2.204	2.221	2.351	2.327
ν_2	3.298	3.390	4.146	4.005
$< E_{2nf} >^1$	-	-	1.607	1.019
$< E_{2nf} >^2$	-	-	1.112	0.752
$< E_3 >$	-	-	2.197	2.220
ν_3	-	-	3.205	3.331
< E >	2.305	2.282	2.388	2.452
ν	4.334	4.348	5.196	5.150

The fig. 5.6 shows the partial contributions of ith-chance fission to the total fission neutron spectrum at incident neutron energy of 14 MeV.

6 Number of neutrons per fission

The number of prompt fission neutrons at thermal energies is calculated by renormalizing Jaffey et al.[34] data to the updated reference values of ν_p: for ^{233}U - 2.485 ±0.008 ; for ^{235}U - 2.414±0.007; for ^{239}Pu - 2.876± 0.009; for

^{252}Cf - 3.757 $\pm$ 0.010. The resulted value of ν_p is 3.429, which is not much different from original value[34]. The energy dependence of ν_p is calculated within Madland-Nix model, the parameters being fixed in Table 5.2.

The comparison with ν_p of JENDL-3 is shown in fig. 6.1

The delayed number of neutrons per fission ν_d is calculated with systematics of Tuttle[35]. Specifically, $\nu_d = 0.00301$ for incident neutron energies up to 6 MeV and $\nu_d = 0.00209$ for higher neutron energies. The decay constants for six groups of delayed neutrons are taken from Brady et al.[36]

7 Angular distributions of secondary neutrons

The angular distributions of elastically scattered neutrons and those for neutrons, scattered on three levels of ground state band are calculated with the coupled channel method. The isotropic compound scattering contribution is taken into account by renormalizing l-th Legendre polynomial coefficients A_l^{cc}, calculated with coupled channels:

$$A_l = A_l^{cc}\sigma_{dir}/(\sigma_{dir}+\sigma_{comp}),$$

where σ_{dir} and σ_{comp} are the scattering cross section direct and compound contributions, respectively. All the other contributing reactions angular distributions of secondary neutrons are assumed isotropic.

8 Conclusions

The evaluated neutron data file for ^{243}Cm is compiled in ENDF/B-VI format and sent to the International Science and Technology Center (Moscow) and Japan Nuclear Data Center at Japan Atomic Energy Research Institute.

The scarcity of experimental data coupled with possibility of some new data becoming available (for example, ^{243}Cm(n,f) data of Fursov et al. (PPEI, Obninsk, Russia) may urge some revision of data file. Present version of ^{243}Cm data file may be revised before March of 1998, the expiration date of Project CIS-03-95.

9 REFERENCES

1. Nakagawa T., Kikuchi Y., Proc. of the Int. Conf. on Nuclear Data and Technology, Gatlinburg, Tenn., USA, 9-13 May, 1994, Dickens J.K. (Editor), 709, ANS Inc., 1994.
2. Bakhanovich L.A., Klepatskij A.B., Maslov V.M., Porodzinskij Yu.V., Sukhovitskij E.Sh., Jadernye Constanty,N 1,p.36,1989
3. Klepatskij A.B., Kolesov A.M., Maslov V.M., Porodzinskij Yu.V., Sukhovitskij E.Sh., INDC(CCP)-316, 1989
4. J.R. Berreth, F.B. Simpson, B.C. Rusche; Nucl. Sci. Eng., 49, 145 (1972).
5. E.K.Hulet, R.W. Hoff, H.R. Bowman, M.C. Michel,Phys. Rev.,107,1294 (1957).
6. V.A. Anufriev, S.I. Babich, N.G. Kochergin, V.M. Lebedev, S.N. Nikolskij, V.N. Nefedov, V.M. Nikolaev, V.A. Poruchikov, A.A. Elesin: Sov. Atomic Energy, 51 (1982) 736
7. Silbert M.G., LA-6239-MS (1976).
8. C.E. Bemis Jr., J.H. Oliver, R. Eby, S. Halperin, Nucl. Sci. Eng., 63, 413 (1977).
9. S.F. Mughabghab: "Neutron Cross Sections, v1, part B", Academic Press (1984).
10. C.L. Dunford: "ENDF Utility Codes Release 6.9", IAEA-NDS-29 (1993)
11. Porodzinskij Yu.V., Sukhovitskij E.Sh., Nuclear Constants, 4, p.27, 1987 (in Russian)
12. Ignatjuk A.V., Istekov K.K., Smirenkin G.N. Sov.J. Nucl. Phys. 29, 450 (1979).
13. Fomushkin E.F., G.F. Novoselov, Y.I. Vinogradov et al., Atomnaya Energiya, 69, 258 (1990).
14. Fomushkin E.F. G.F. Novoselov, Y.I. Vinogradov et al., Atomnaya Energiya, 62, 278 (1987).
15. Fursov B.I., Samylin B.F., Smirenkin G.N., et al. Nuclear Data for Science and Technology, Proc. Int.Conf., Gatlinburg, 1994, 269, ANS.
16. Haouat, Lachkar J., Lagrange Ch., et al., Nucl.Sci. Engng. 81, 491 (1982)
17. Klepatskij A.B., Sukhovitskij E.Sh., private communication.
18. Ellis-Akovali Y.A., Nucl. Data Sheets, 44, 407 (1985)
19. Fullwood R.R., Dixon D.R., Lougheed R.W. LA-4420, 1970
20. Maslov, Ann. Nucl. Energy, 20, 163 (1993).
21. Howard W.M., Moller P. Atomic Data and Nuclear Data Tables,25, 219 (1980)
22. Ignatjuk A.V., Maslov V.M., Proc. Int. Symp. Nuclear Data Evaluation Methodology, Brookhaven,USA, October 12-16, 1992, p.440, World

Scientific, 1993.
23. Tepel J.W., Hoffman H.M., Weidenmuller H.A. Phys. Lett. 49, 1 (1974).
24. Ignatjuk A.V., Maslov V.M., Pashchenko A.B. Sov. J. Nucl. Phys. 47, 224 (1988).
25. Fomushkin E.F., Novoselov G.F., Gavrilov G.F. et al.,in: Nuclear Data for Science and Technology (Springer-Verlag,1992), p.439.
26.Uhl M. and Strohmaier B., Report IRK - 76/10 (Vienna,1976).
27. Maslov V.M., Porodzinskij Yu.V.,Sukhovitskij E.Sh., Proc. Int. Conf. on Neutron Physics, 14-18 Sept., Kiev, USSR, V.1, p.413, 1988.
28. Madland D.G., Nix J.R., Nucl. Sci. Engng. 81, 213 (1982).
29. Dickens J.K. Nucl.Sci. Engng. 96, 8 (1987).
30. Wapstra A.H. et al. At. Data & Nucl. Data Tables, 39, 281 (1988).
31. Viola V.E., Kwiatkowski K., Walker M., Phys. Rev., 31, 1550 (1985).
32. Becchetti F.D., Greenlees G.W., Phys. Rev. 182, 1190 (1969).
33. Zhuravlev K.D., Zamyatnin Yu.S., Kroshkin N.I., Neutron Physics, Proc. of 2nd Conf. on Neutron Physics, v.4, 57 (1975).
34. Jaffey A.H., Lerner J.L., Nucl. Phys. A, 145, 1 (1970).
35. Tuttle R.J. Proc. Consultants Meeting on Delayed Neutron Properties, 1979, Vienna, INDC(NDS)-107/G, p.29.
36. Brady M.C., Wright R.Q. , England T.R. Report ORNL/CSD/TM-226(1991),IAEA-NDS-102, 1992

10 Figure captions

Fig. 2.1 Total cross section of ^{243}Cm in the energy region 14-25 eV.
Fig. 2.2 Fission cross section of ^{243}Cm in the energy region 14-25 eV.
Fig. 2.3 Total cross section of ^{243}Cm in the energy region 25-40 eV.
Fig. 2.4 Fission cross section of ^{243}Cm in the energy region 25-40 eV.
Fig. 2.5 Total cross section of ^{243}Cm in the energy region 40-55 eV.
Fig. 2.6 Fission cross section of ^{243}Cm in the energy region 40-55 eV.
Fig. 2.7 Total cross section of ^{243}Cm in the energy region 55-70 eV.
Fig. 2.8 Fission cross section of ^{243}Cm in the energy region 55-70 eV.
Fig. 2.9 Fission cross section of ^{243}Cm in the energy region 70-100 eV.
Fig. 3.1 Distribution of reduced neutron widths for ^{243}Cm.
Fig. 3.2 Neutron resonance spacing distribution for ^{243}Cm.
Fig. 3.3 Comparison of reduced neutron widths distributions for two energy intervals.
Fig. 3.4 Comparison of neutron resonance spacing distributions for two energy intervals.
Fig. 3.5 Fission cross section of ^{243}Cm in unresolved resonance region.
Fig. 3.6 Radiation capture cross section of ^{243}Cm in unresolved resonance region.
Fig. 4.1 Compound reaction cross section of ^{243}Cm.
Fig. 4.2 Total cross section of ^{243}Cm.
Fig. 4.3 Elastic scattering cross section of ^{243}Cm.
Fig. 4.4 Fission cross section of ^{243}Cm
Fig. 4.5 Fission cross section of ^{243}Cm
Fig. 4.6 Fission cross section of ^{243}Cm
Fig. 4.7 Cumulative number of levels of ^{243}Cm
Fig. 4.8 Inelastic scattering cross section of ^{243}Cm.
Fig. 4.9 Cross section of ^{243}Cm: 0.042 MeV, $7/2^+$ level excitation.
Fig. 4.10 Cross section of ^{243}Cm: 0.0939 MeV, $9/2^+$ level excitation.
Fig. 4.11 Cross section of ^{243}Cm: 0.153 MeV, $11/2^+$ level excitation.
Fig. 4.12 Cross section of ^{243}Cm: 0.219 MeV, $13/2^+$ level excitation.
Fig. 4.13 Cross section of ^{243}Cm: 0.3 MeV, $15/2^+$ level excitation.
Fig. 4.14 Radiative capture cross section of ^{243}Cm.
Fig. 4.15 ^{243}Cm(n,2n) reaction cross section
Fig. 4.16 ^{243}Cm(n,3n) reaction cross section
Fig. 5.1 First neutron spectra of ^{243}Cm for incident neutron energy 14 MeV.
Fig. 5.2 Second neutron spectra of ^{243}Cm for incident neutron energy 14 MeV.
Fig. 5.3 Third neutron spectra of ^{243}Cm for incident neutron energy 14

MeV.
Fig. 5.4 Prompt fission neutron spectrum of ^{243}Cm for thermal incident neutron energy as ratio to JENDL-3 evaluation (T_{max} = 1.408 MeV).
Fig. 5.5 Thermal prompt fission neutron spectrum.
Fig. 5.6 Fission neutron spectra of ^{243}Cm for incident neutron energy 14 MeV.
Fig. 6.1 Prompt fission neutron multiplicity of ^{243}Cm.

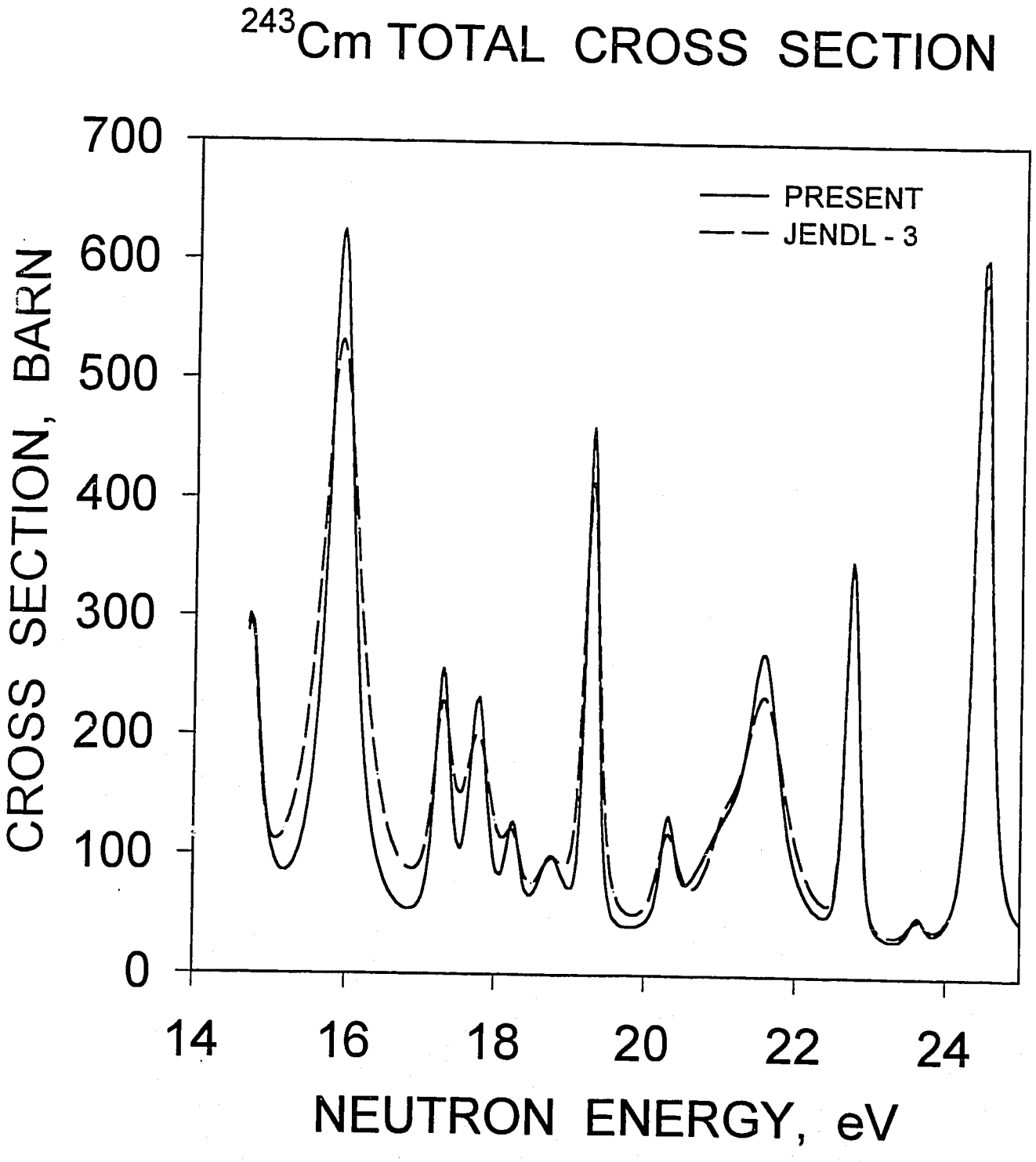
^{243}Cm TOTAL CROSS SECTION
PRESENT
JENDL - 3
CROSS SECTION, BARN
700
600
500
400
300
200
100
0
14
16
18
20
22
24
NEUTRON ENERGY, eV

FIG. 2.1

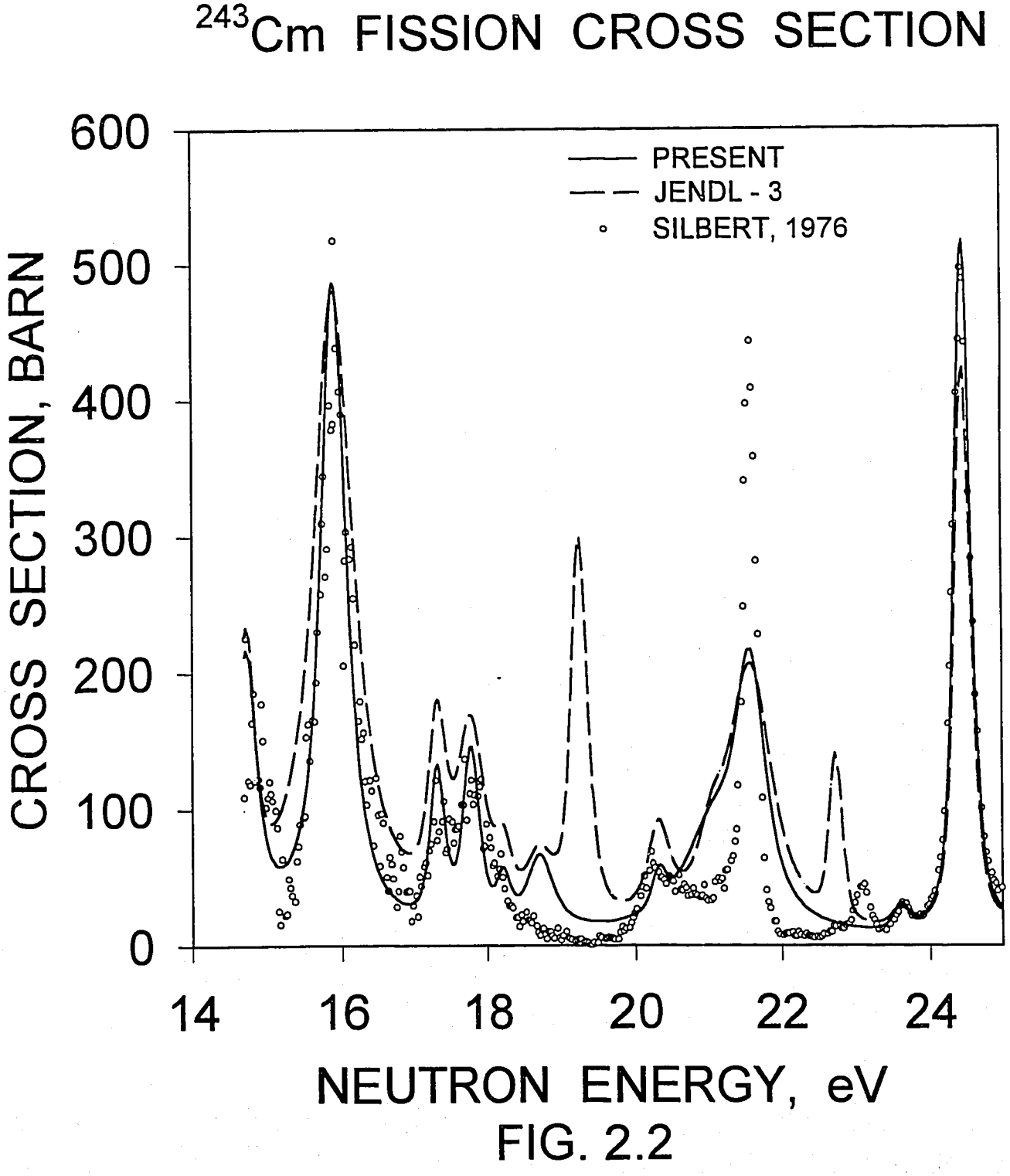
^{243}Cm FISSION CROSS SECTION
PRESENT
JENDL - 3
SILBERT, 1976
CROSS SECTION, BARN
600
500
400
300
200
100
0
14
16
18
20
22
24
NEUTRON ENERGY, eV

FIG. 2.2

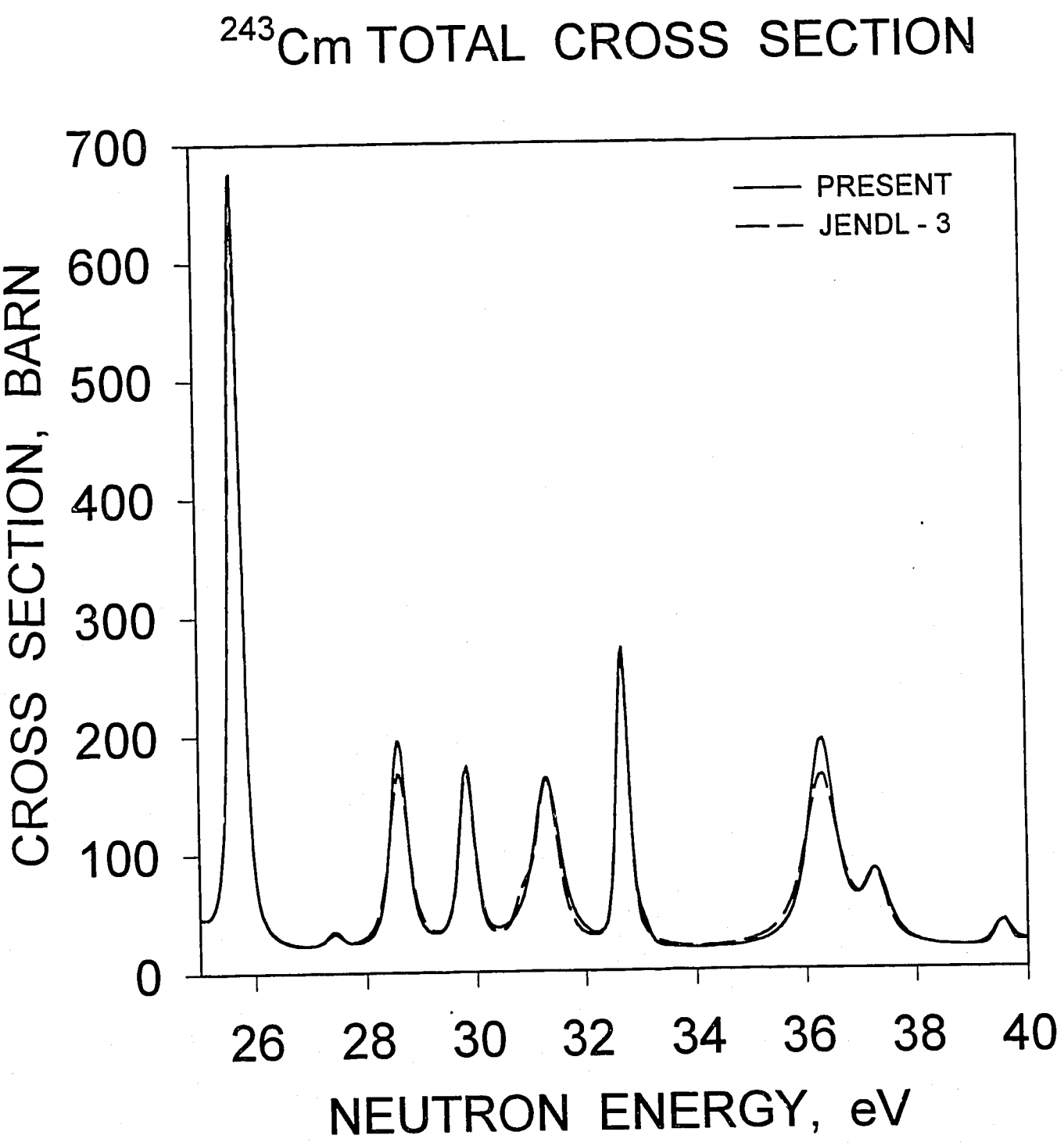
^{243}Cm TOTAL CROSS SECTION
PRESENT
JENDL - 3
CROSS SECTION, BARN
700
600
500
400
300
200
100
0
26
28
30
32
34
36
38
40
NEUTRON ENERGY, eV

FIG. 2.3

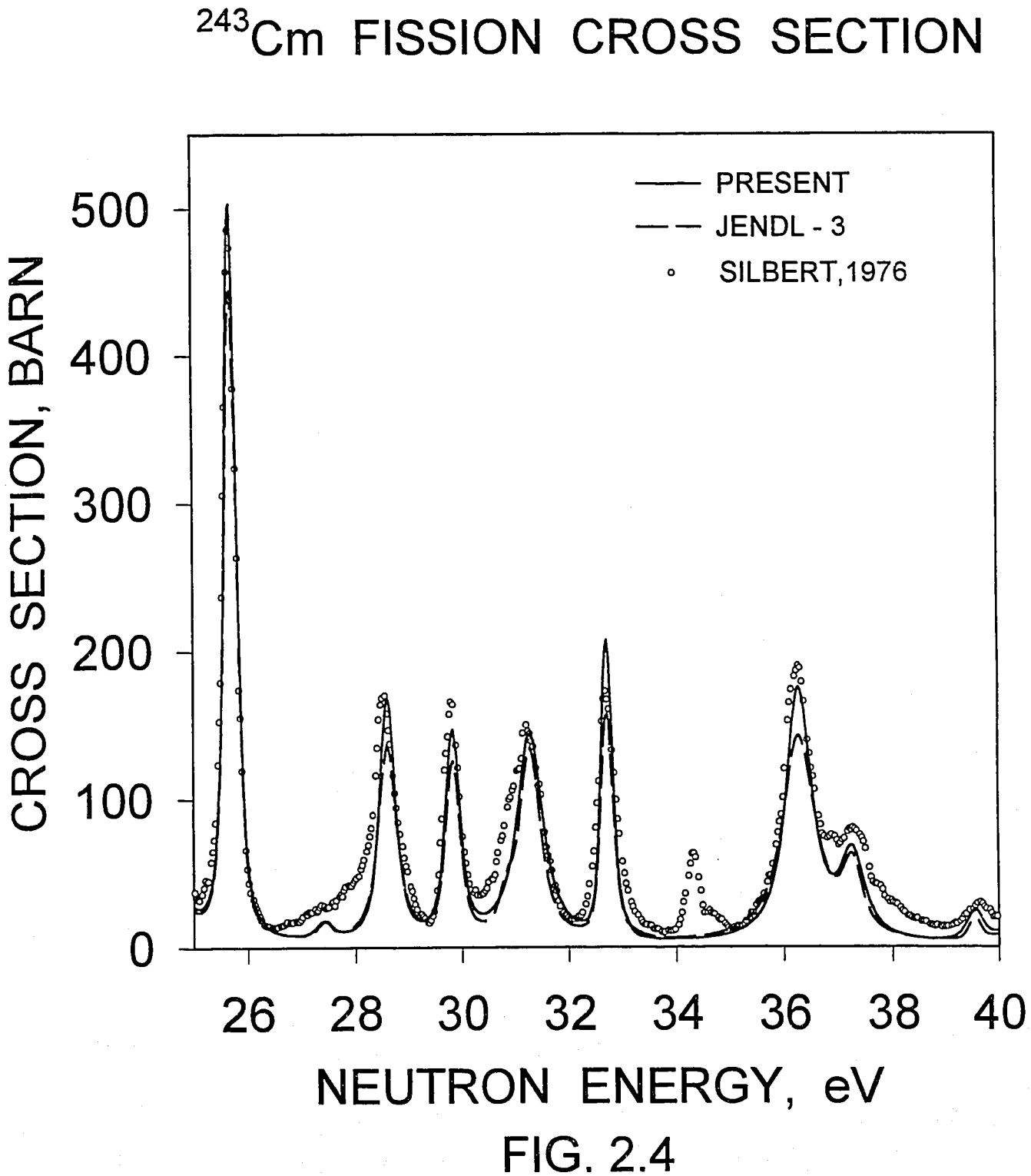
^{243}Cm FISSION CROSS SECTION
PRESENT
JENDL - 3
SILBERT,1976
CROSS SECTION, BARN
0
100
200
300
400
500
26
28
30
32
34
36
38
40
NEUTRON ENERGY, eV

FIG. 2.4

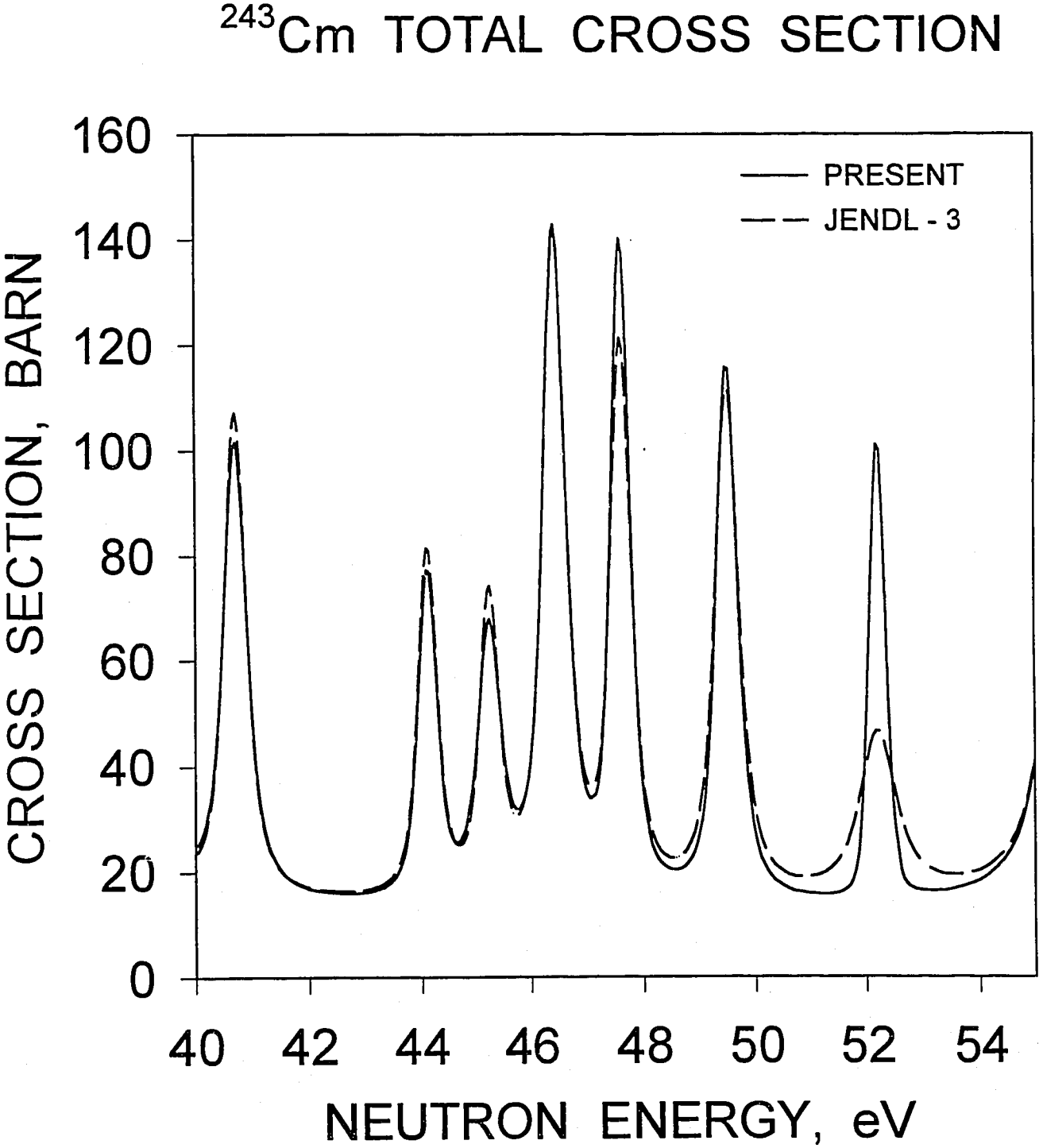
^{243}Cm TOTAL CROSS SECTION
PRESENT
JENDL - 3
CROSS SECTION, BARN
160
140
120
100
80
60
40
20
0
40
42
44
46
48
50
52
54
NEUTRON ENERGY, eV

FIG. 2.5

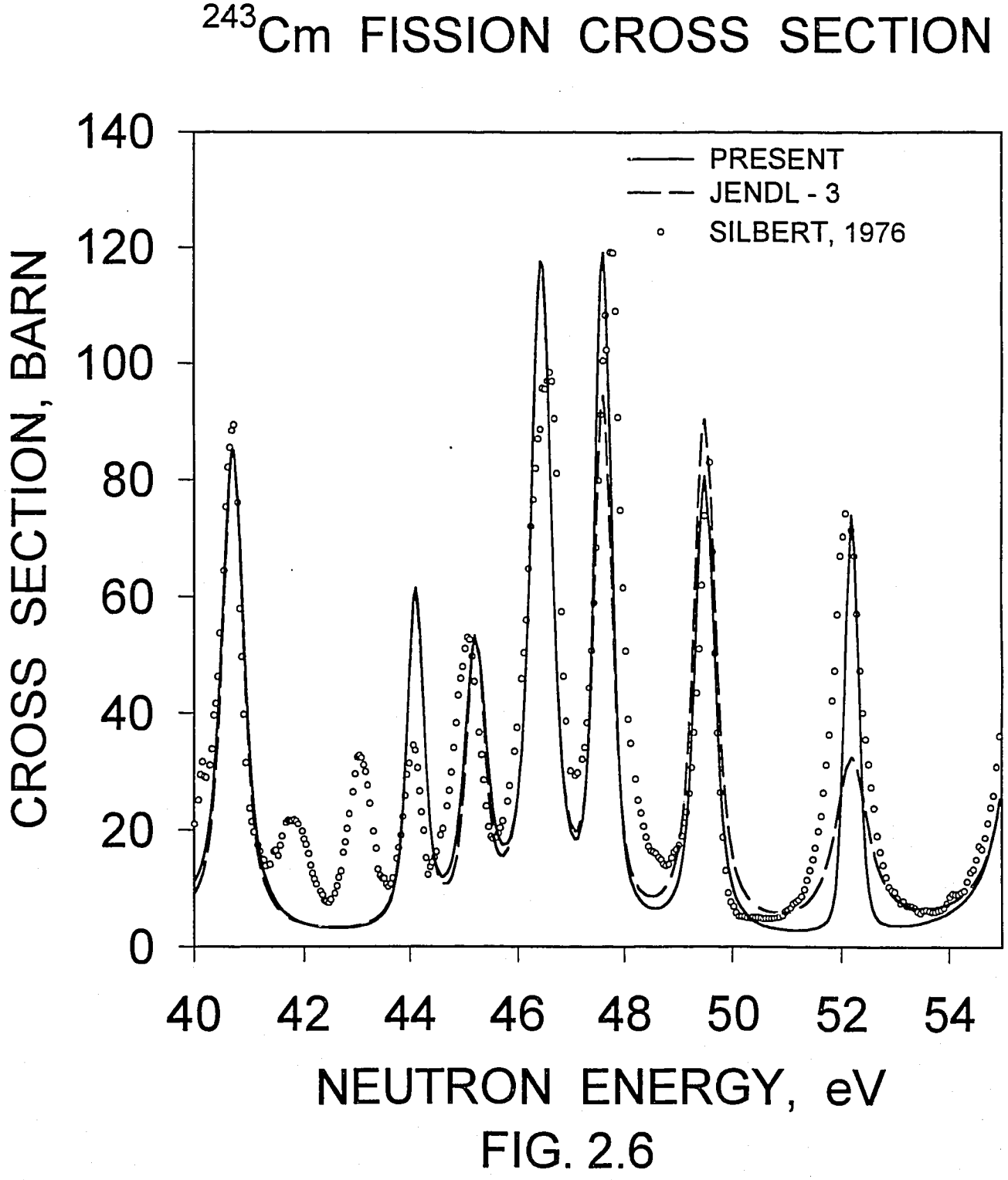
^{243}Cm FISSION CROSS SECTION
PRESENT
JENDL - 3
SILBERT, 1976
CROSS SECTION, BARN
0
20
40
60
80
100
120
140
40
42
44
46
48
50
52
54
NEUTRON ENERGY, eV

FIG. 2.6

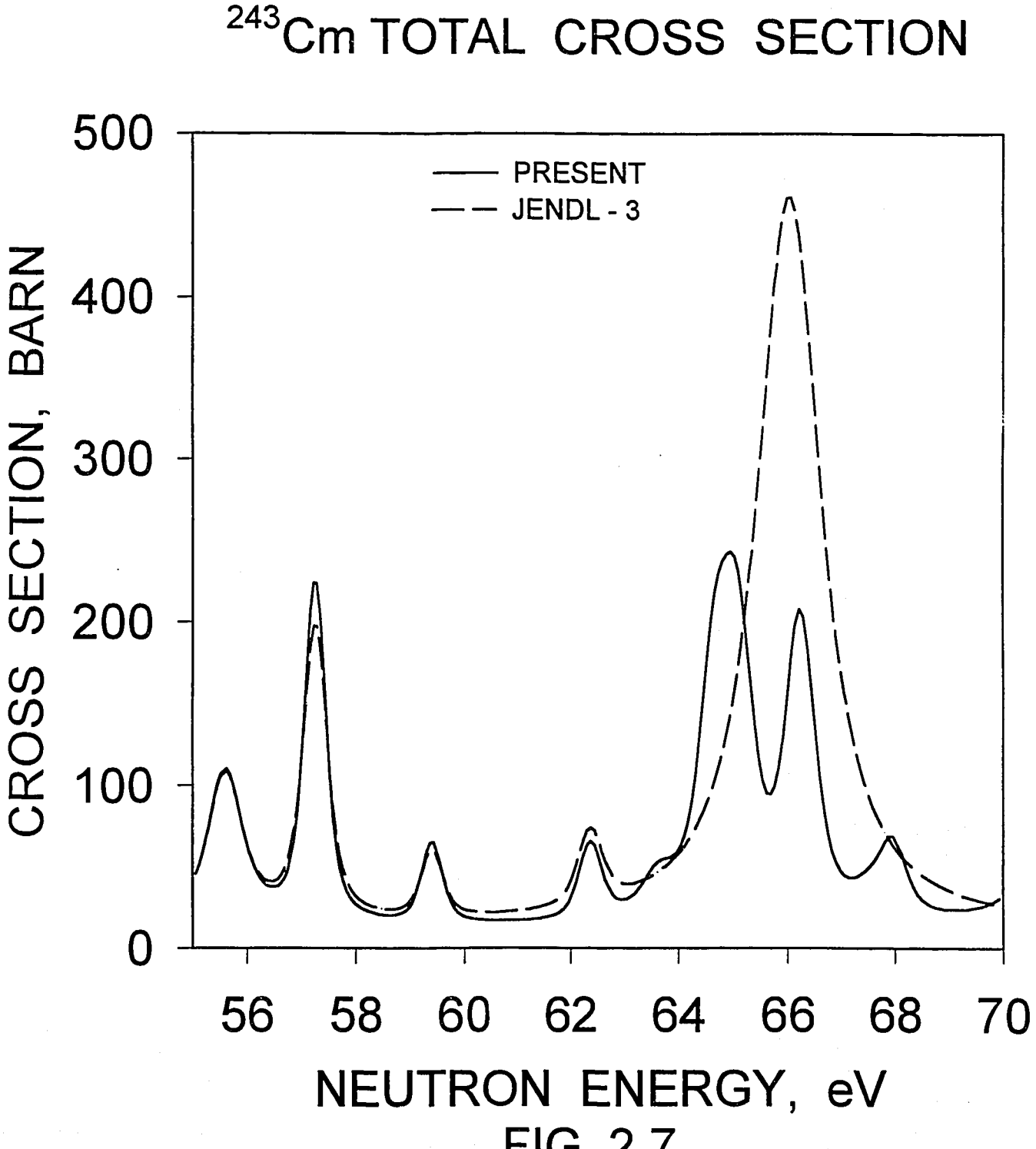
^{243}Cm TOTAL CROSS SECTION
PRESENT
JENDL - 3
CROSS SECTION, BARN
500
400
300
200
100
0
56
58
60
62
64
66
68
70
NEUTRON ENERGY, eV

FIG. 2.7

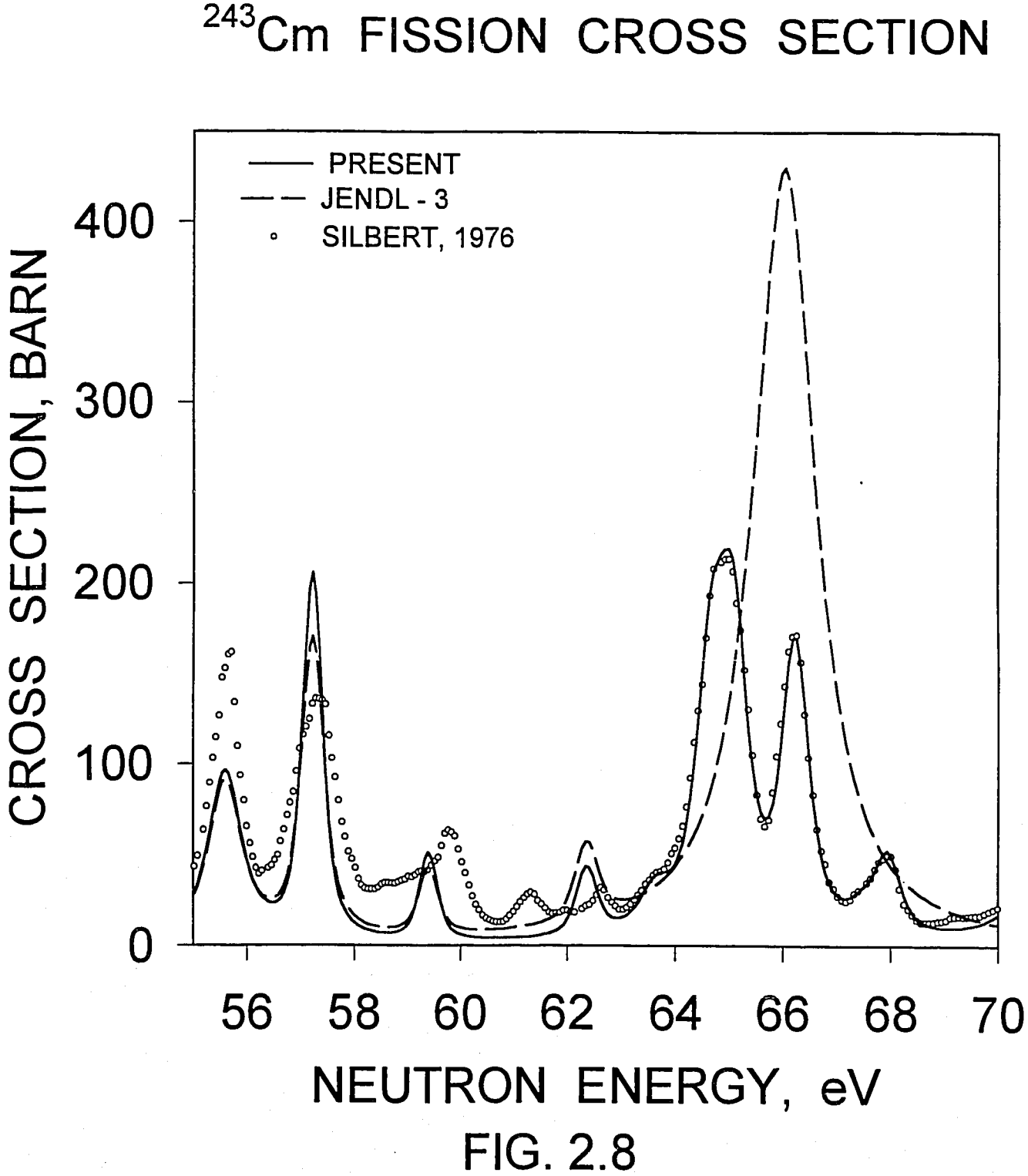
^{243}Cm FISSION CROSS SECTION
PRESENT
JENDL - 3
SILBERT, 1976
CROSS SECTION, BARN
0
100
200
300
400
56
58
60
62
64
66
68
70
NEUTRON ENERGY, eV

FIG. 2.8

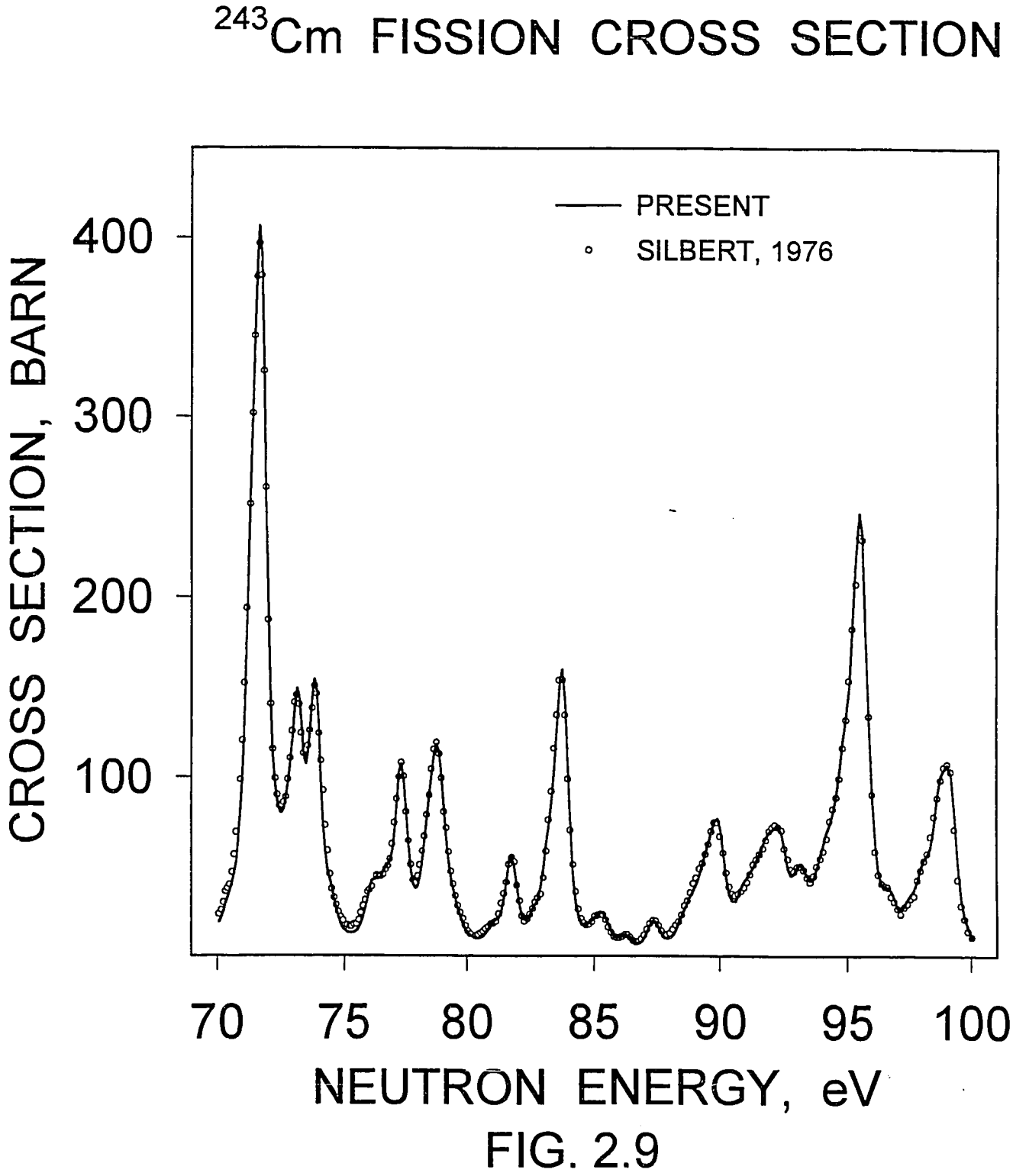
^{243}Cm FISSION CROSS SECTION
PRESENT
SILBERT, 1976
CROSS SECTION, BARN
400
300
200
100
70
75
80
85
90
95
100
NEUTRON ENERGY, eV

FIG. 2.9

^{243}Cm NEUTRON WIDTHS DISTRIBUTION

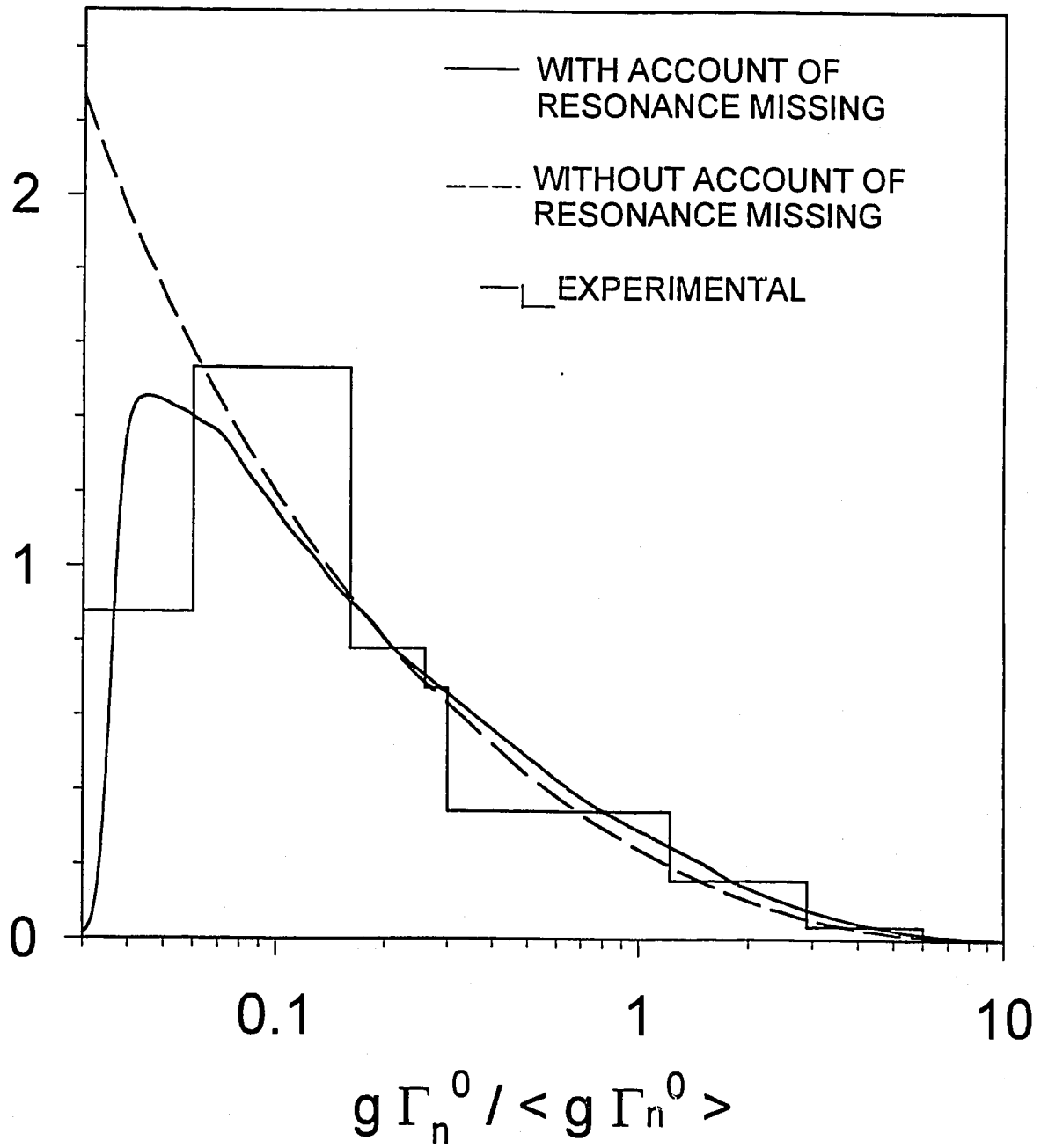

FIG. 3.1

^{243}Cm RESONANCE SPACING DISTRIBUTION

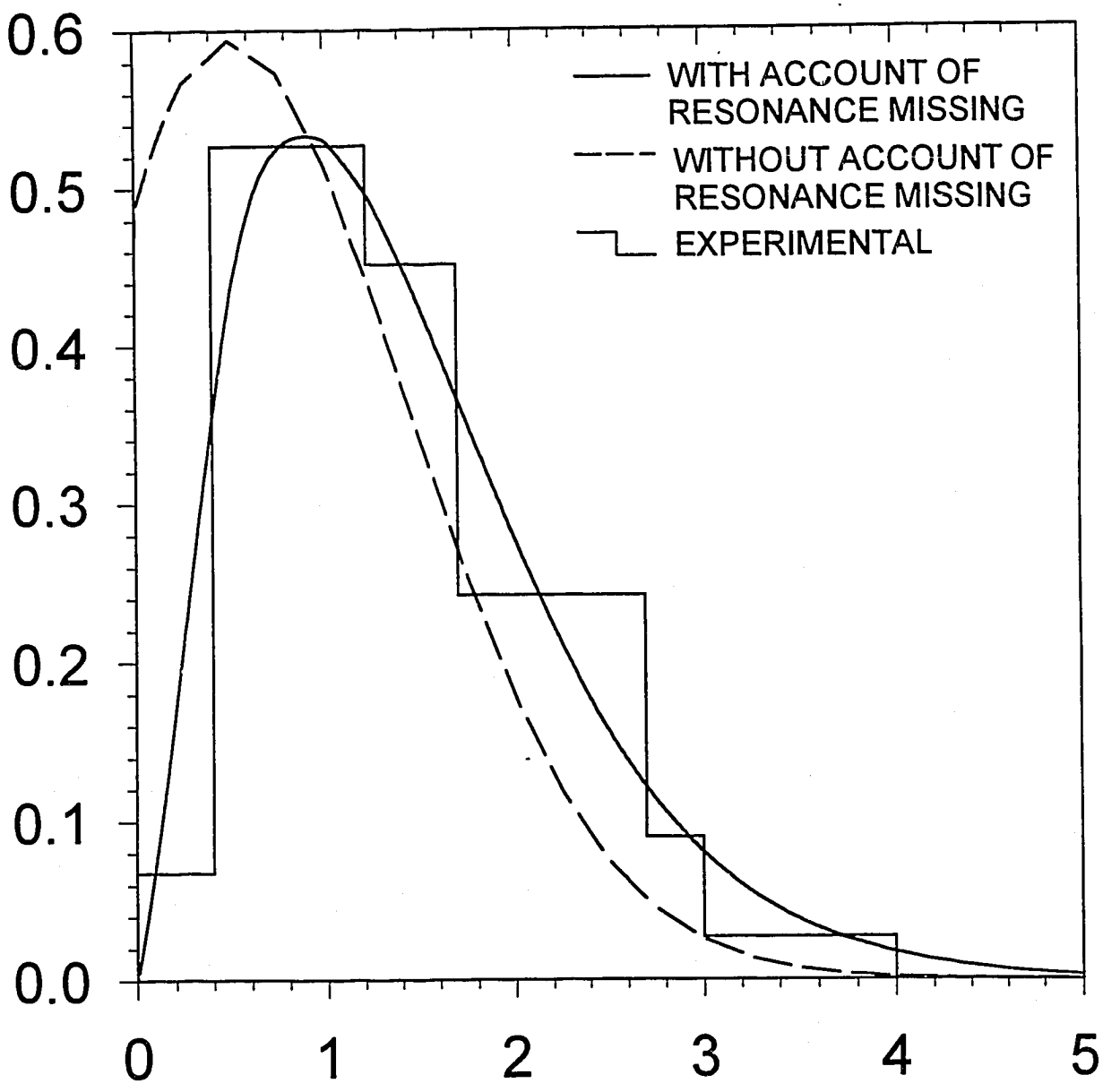

FIG. 3.2

^{243}Cm NEUTRON WIDTHS DISTRIBUTION

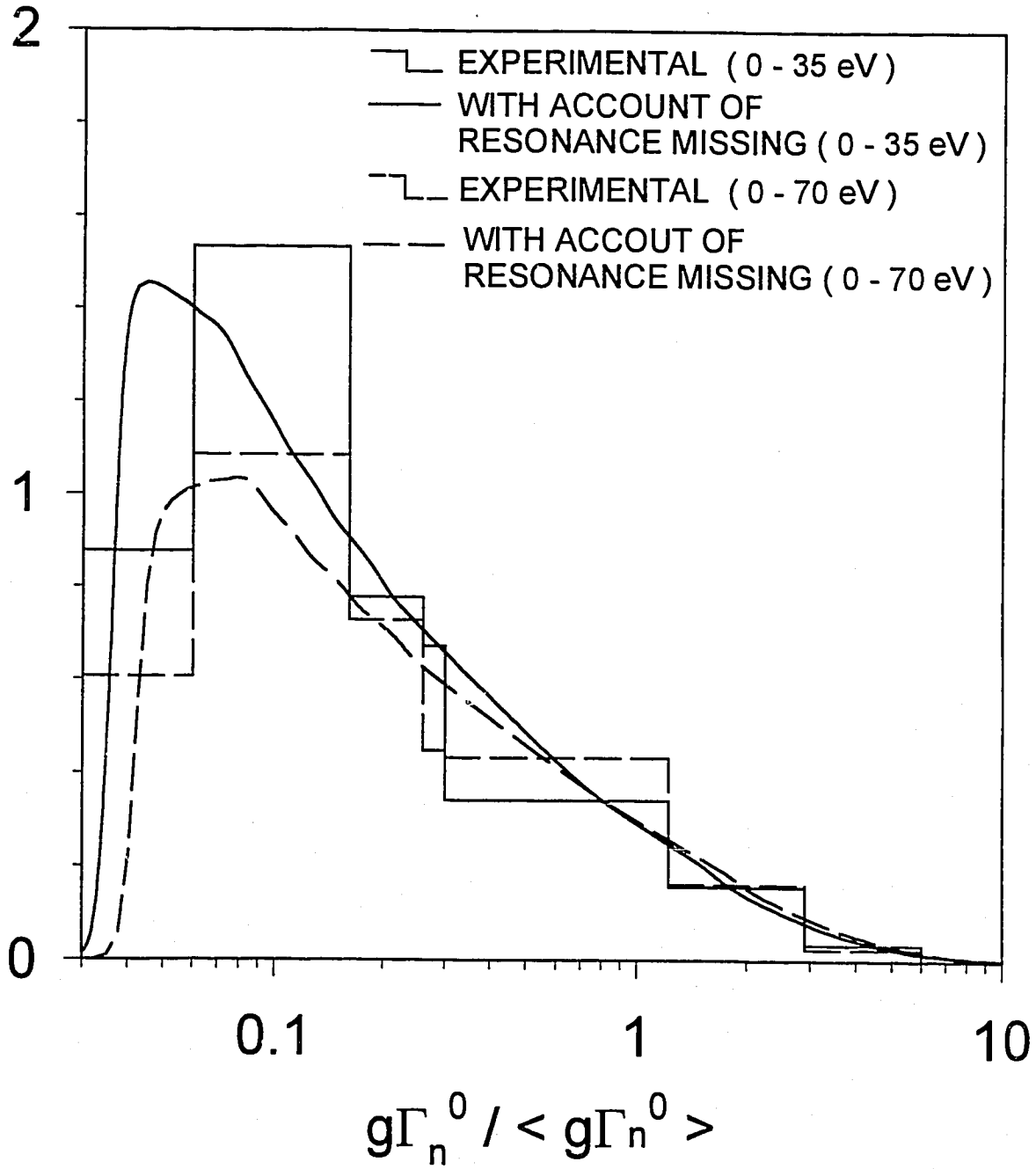

FIG. 3.3

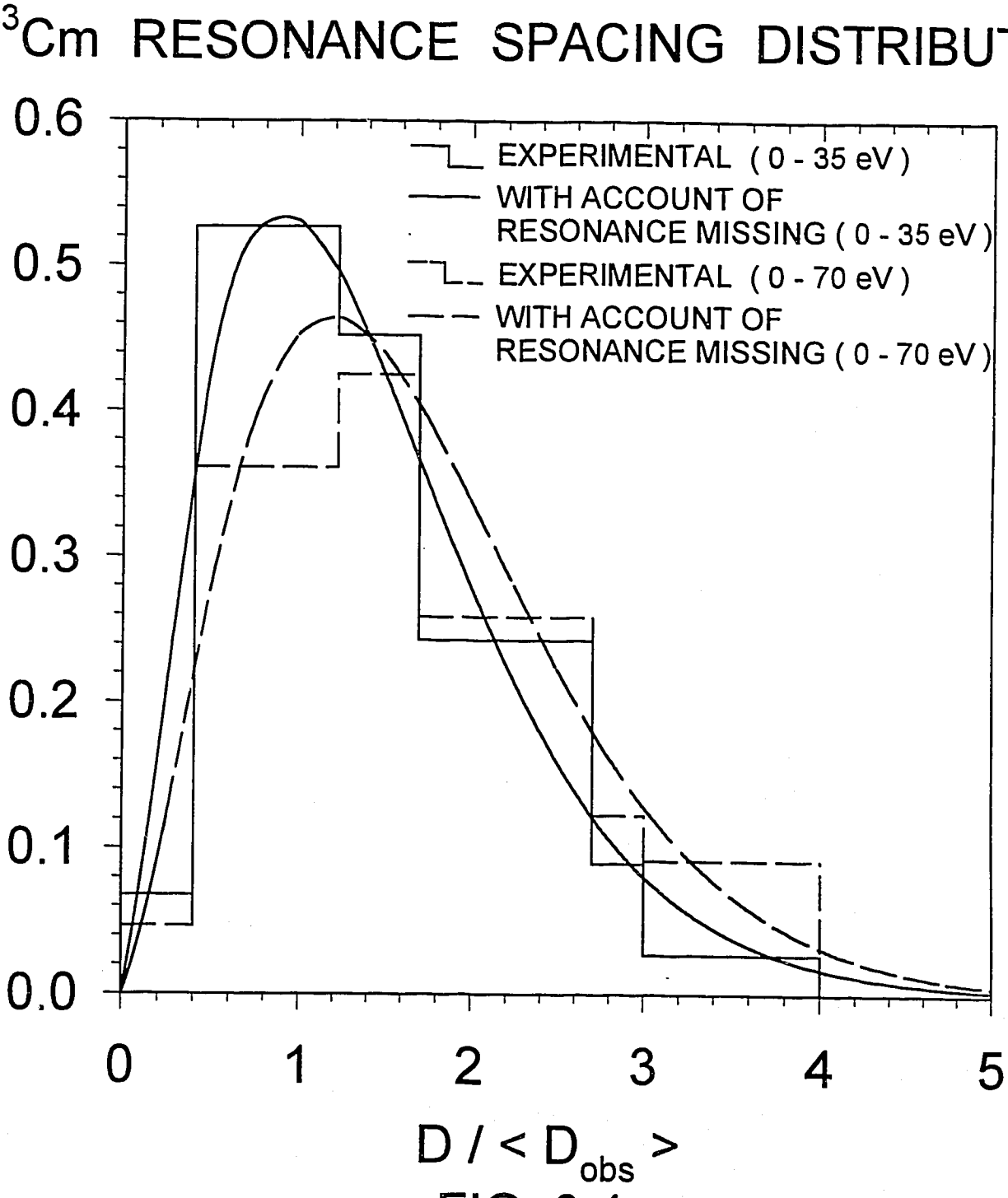
^{243}Cm RESONANCE SPACING DISTRIBUTION
EXPERIMENTAL (0 - 35 eV)
WITH ACCOUNT OF RESONANCE MISSING (0 - 35 eV)
EXPERIMENTAL (0 - 70 eV)
WITH ACCOUNT OF RESONANCE MISSING (0 - 70 eV)
0.6
0.5
0.4
0.3
0.2
0.1
0.0
0
1
2
3
4
5
D / < D$_{obs}$ >

FIG. 3.4

^{243}Cm FISSION CROSS SECTION ^{243}Cm

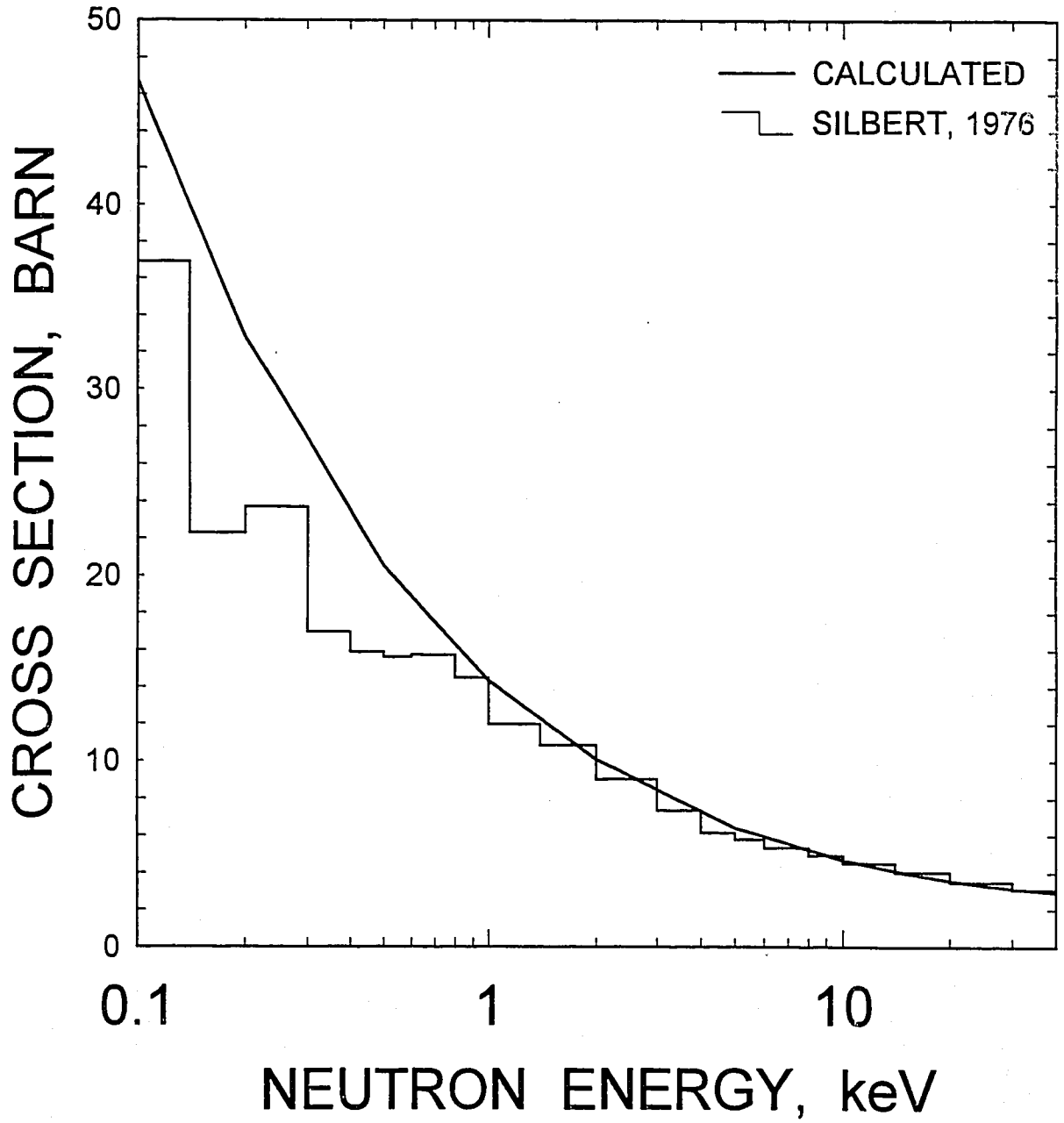

FIG. 3.5

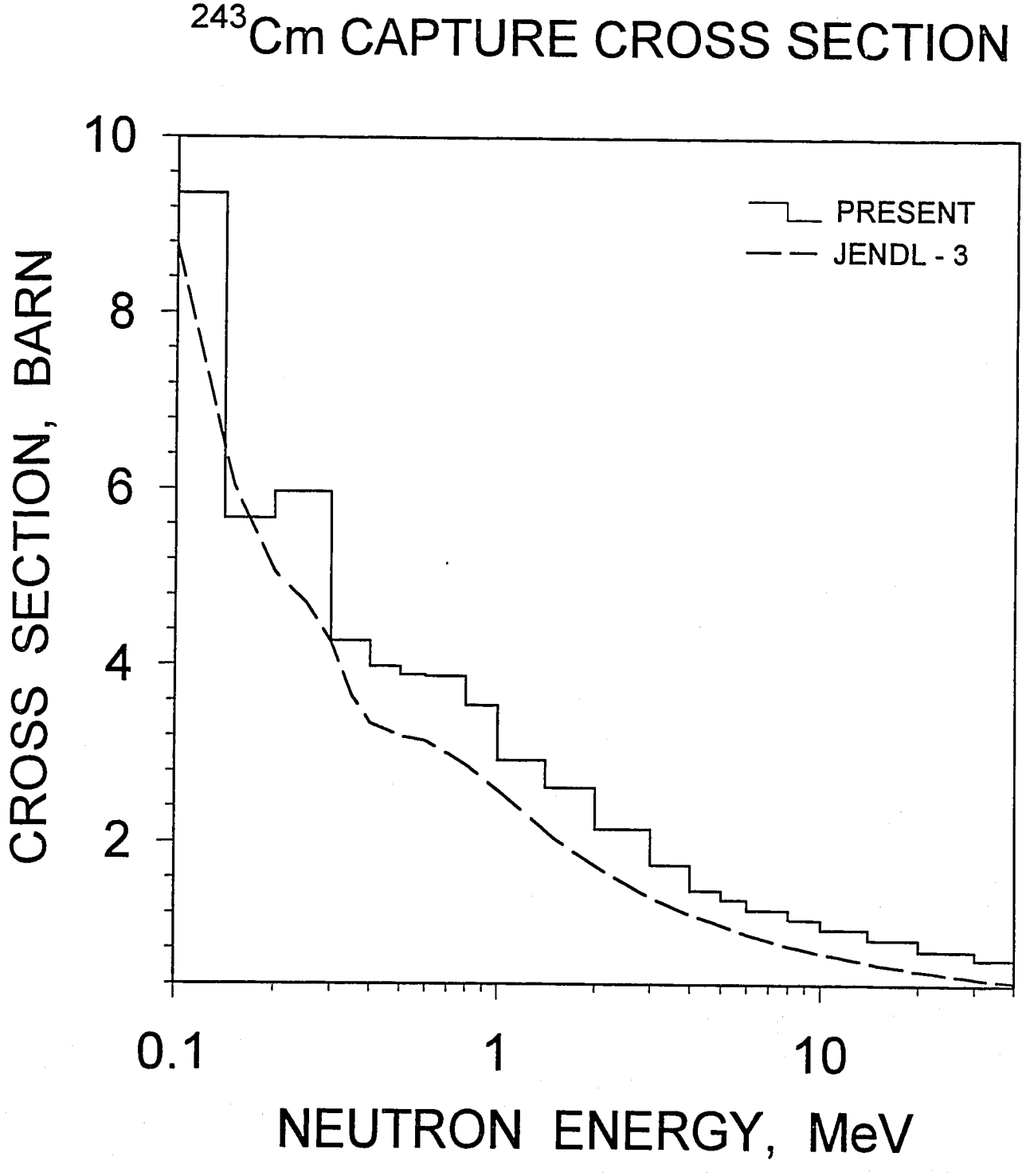
^{243}Cm CAPTURE CROSS SECTION
CROSS SECTION, BARN
10
8
6
4
2
PRESENT
JENDL - 3
0.1
1
10
NEUTRON ENERGY, MeV

FIG. 3.6

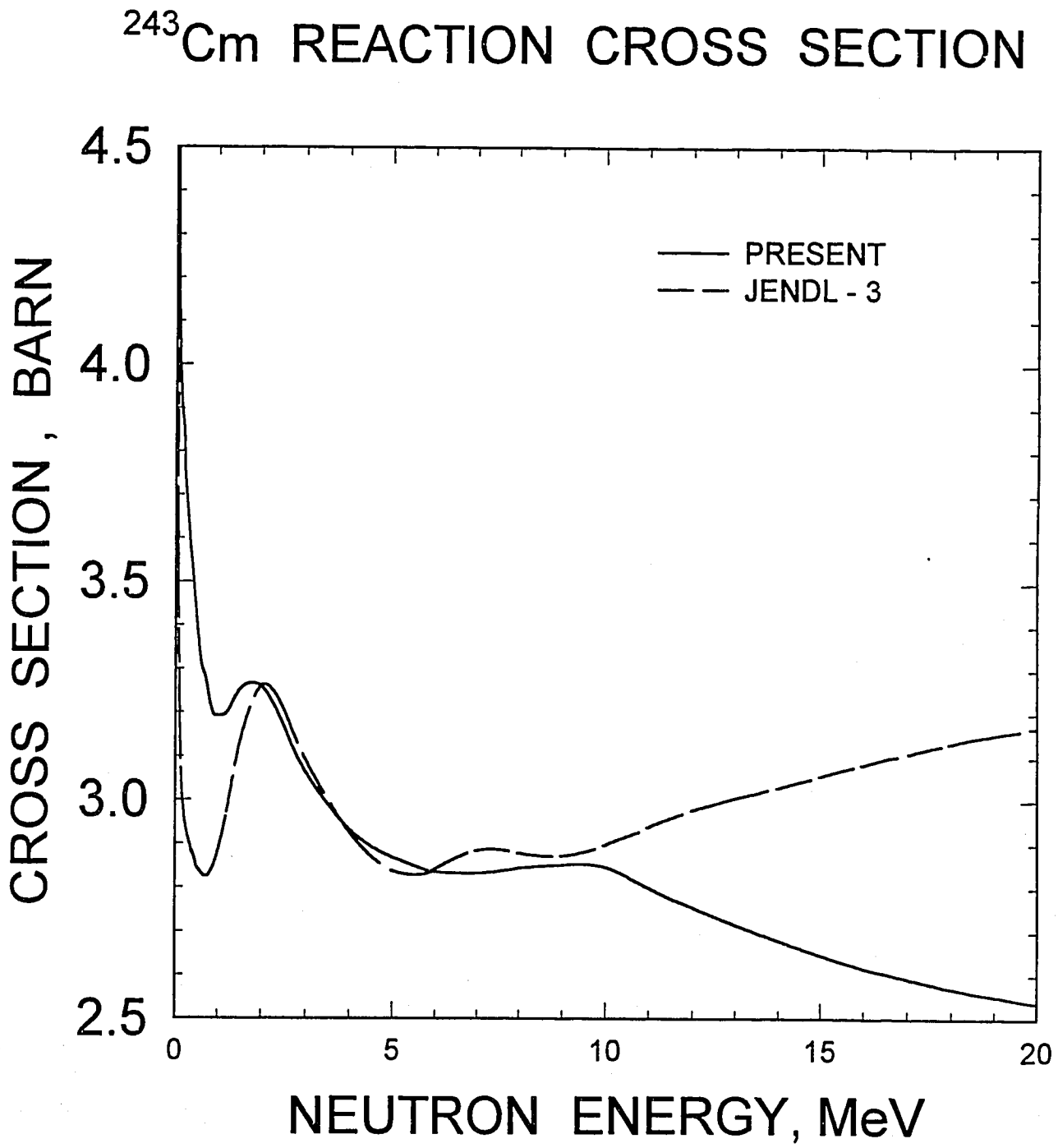
^{243}Cm REACTION CROSS SECTION
CROSS SECTION , BARN
4.5
4.0
3.5
3.0
2.5
0
5
10
15
20
NEUTRON ENERGY, MeV
PRESENT
JENDL - 3

FIG. 4.1

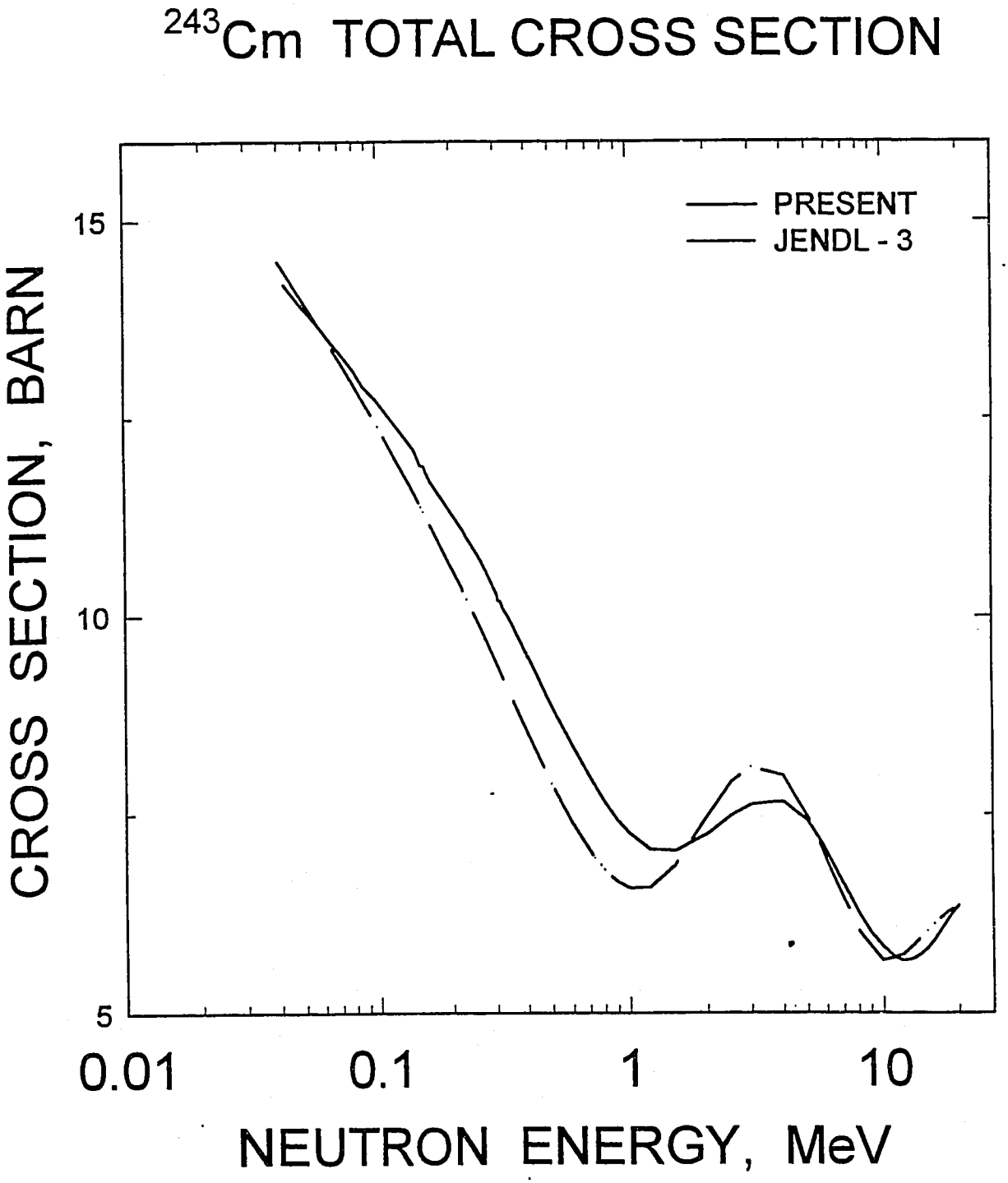
^{243}Cm TOTAL CROSS SECTION
PRESENT
JENDL - 3
CROSS SECTION, BARN
15
10
5
0.01
0.1
1
10
NEUTRON ENERGY, MeV

FIG. 4.2

^{243}Cm ELASTIC SCATTERING CROSS SECTION

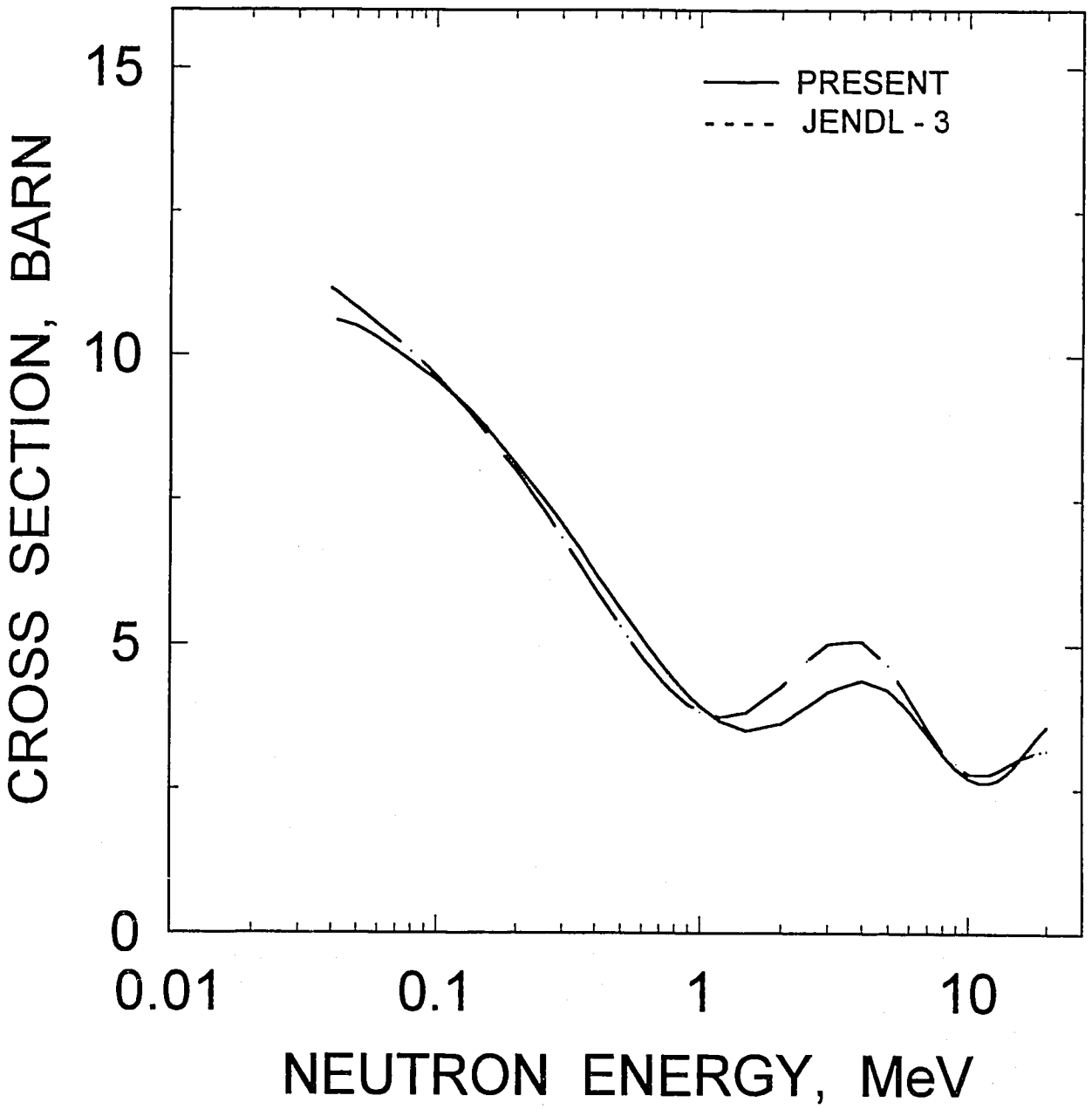

FIG. 4.3

^{243}Cm FISSION CROSS SECTION

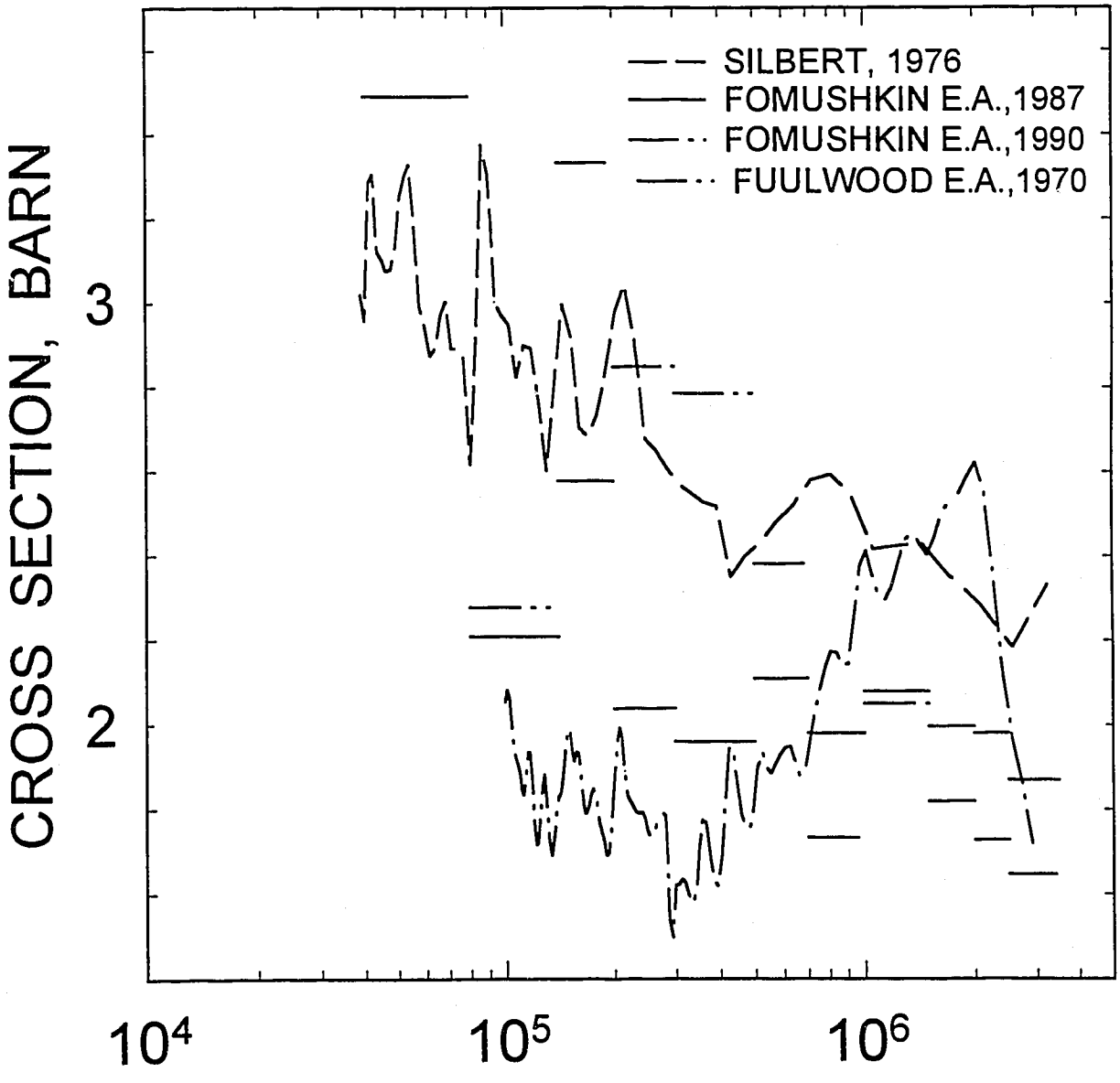

FIG. 4.4

^{243}Cm FISSION CROSS SECTION

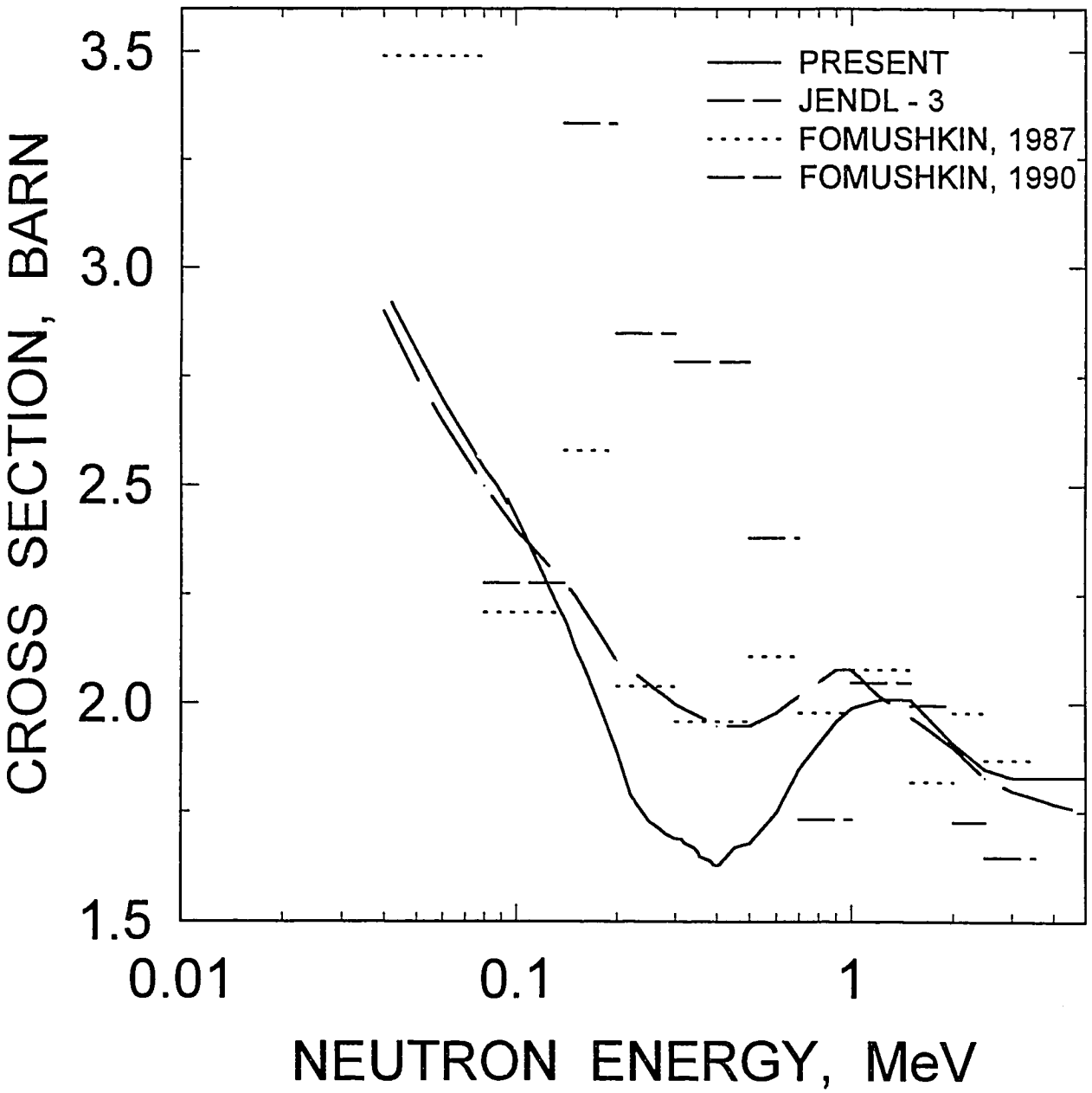

FIG. 4.5

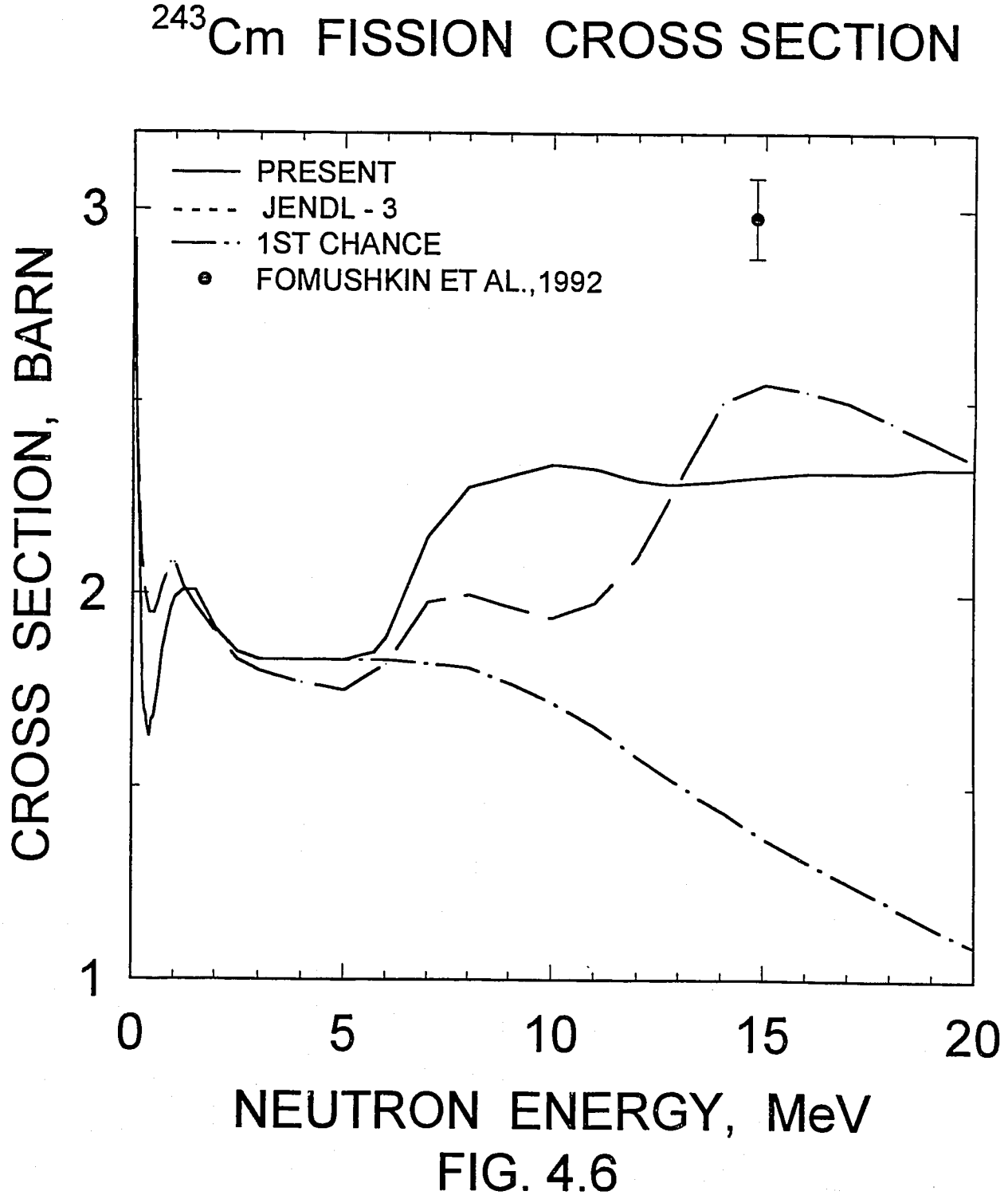
^{243}Cm FISSION CROSS SECTION
PRESENT
JENDL - 3
1ST CHANCE
FOMUSHKIN ET AL.,1992
CROSS SECTION, BARN
1
2
3
0
5
10
15
20
NEUTRON ENERGY, MeV

FIG. 4.6

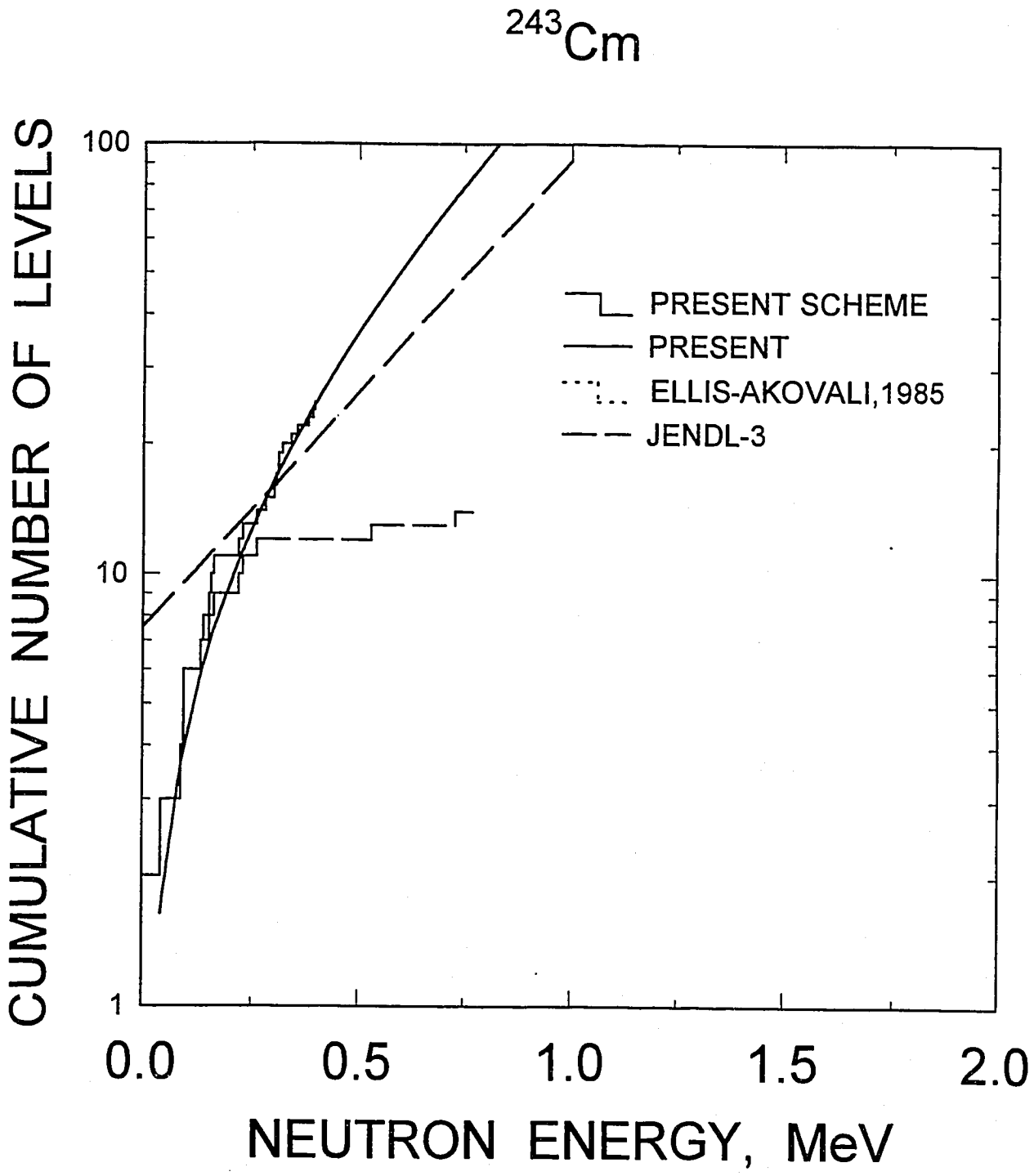
^{243}Cm
CUMULATIVE NUMBER OF LEVELS
100
10
1
0.0
0.5
1.0
1.5
2.0
NEUTRON ENERGY, MeV
PRESENT SCHEME
PRESENT
ELLIS-AKOVALI,1985
JENDL-3

FIG. 4.7

^{243}Cm TOTAL INELASTIC CROSS SECTION

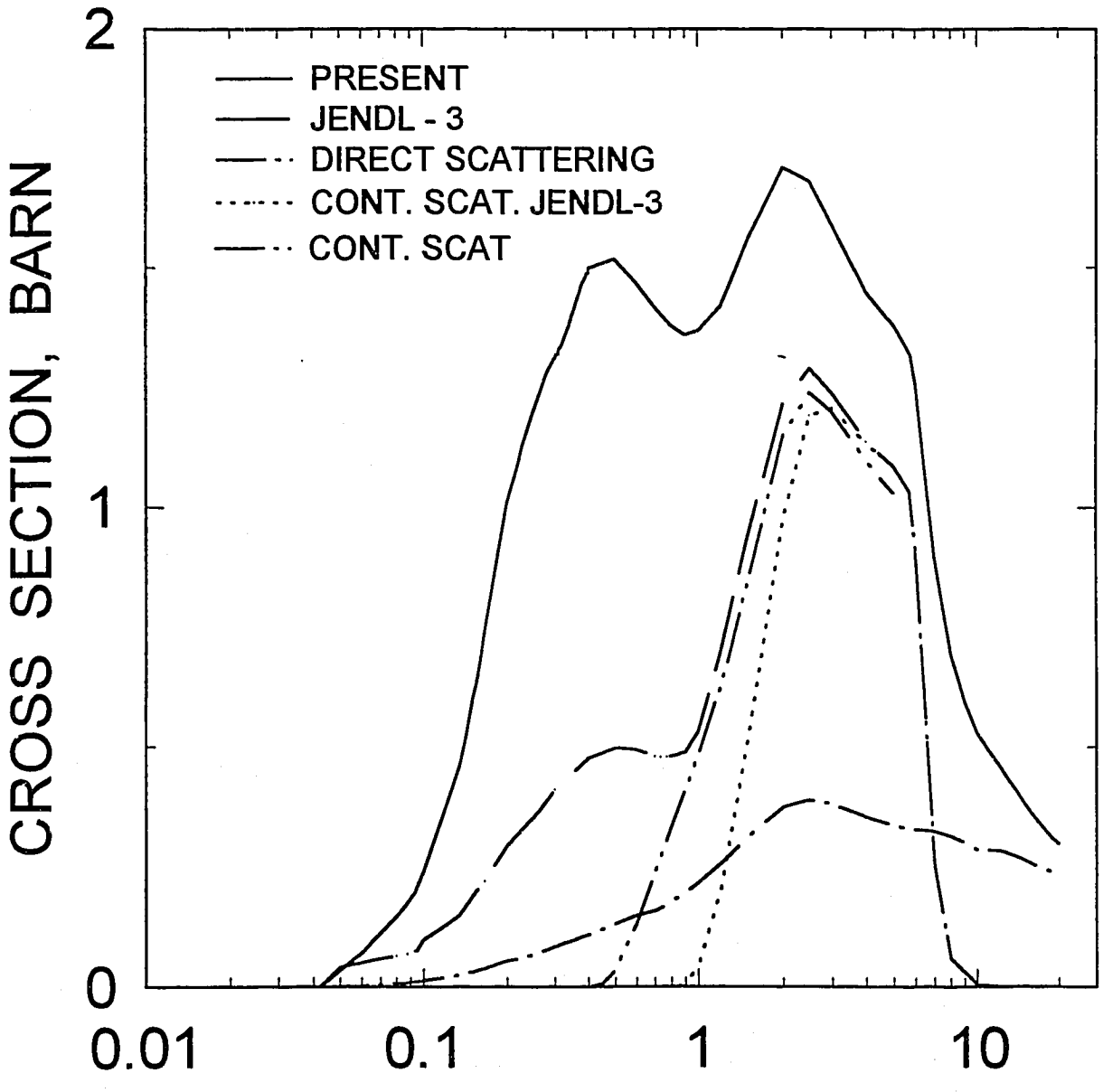

FIG. 4.8

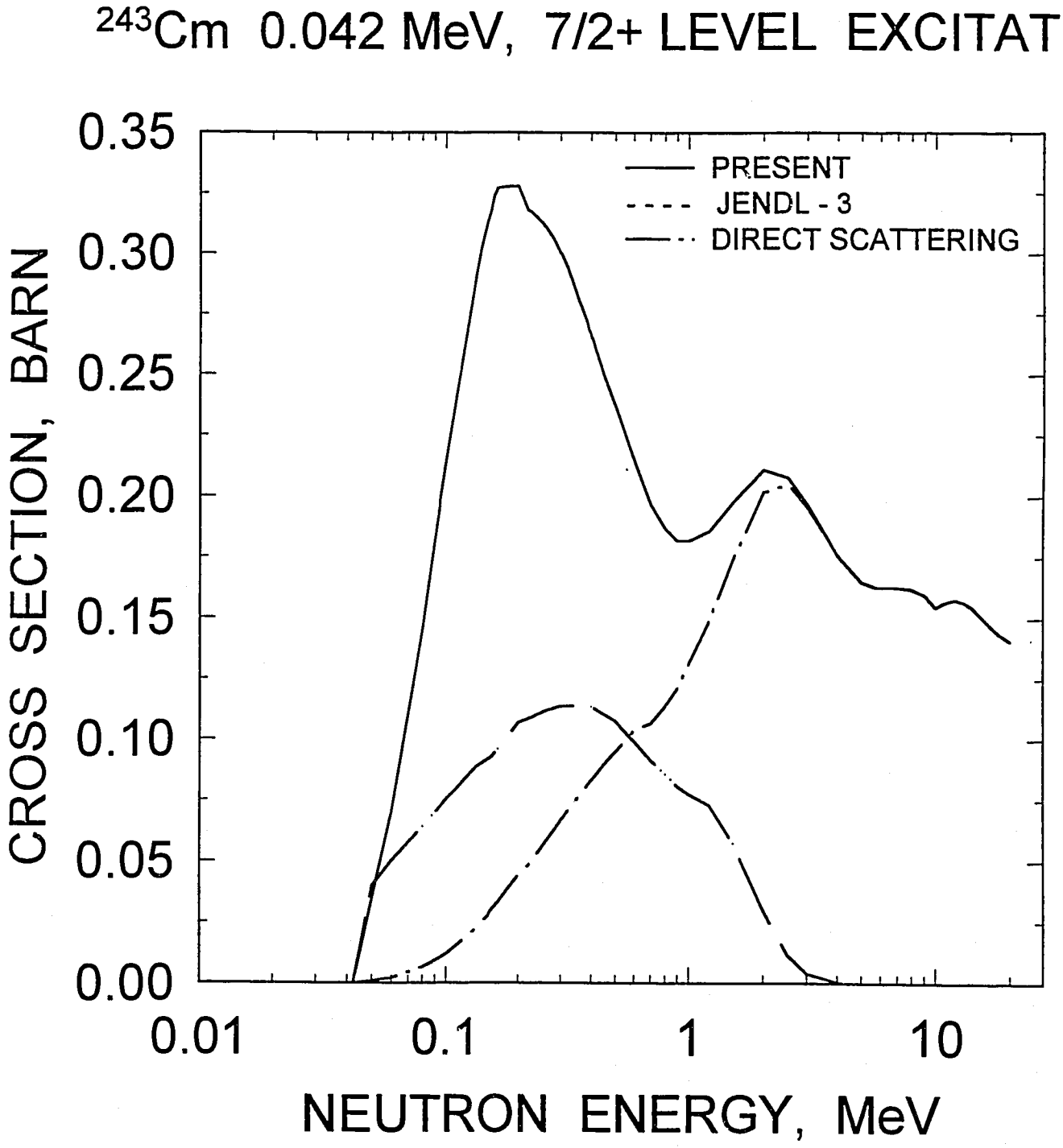
^{243}Cm 0.042 MeV, 7/2+ LEVEL EXCITATION
PRESENT
JENDL - 3
DIRECT SCATTERING
CROSS SECTION, BARN
0.35
0.30
0.25
0.20
0.15
0.10
0.05
0.00
0.01
0.1
1
10
NEUTRON ENERGY, MeV

FIG. 4.9

^{243}Cm: 0.0939 MeV, 9/2+ LEVEL EXCITATION

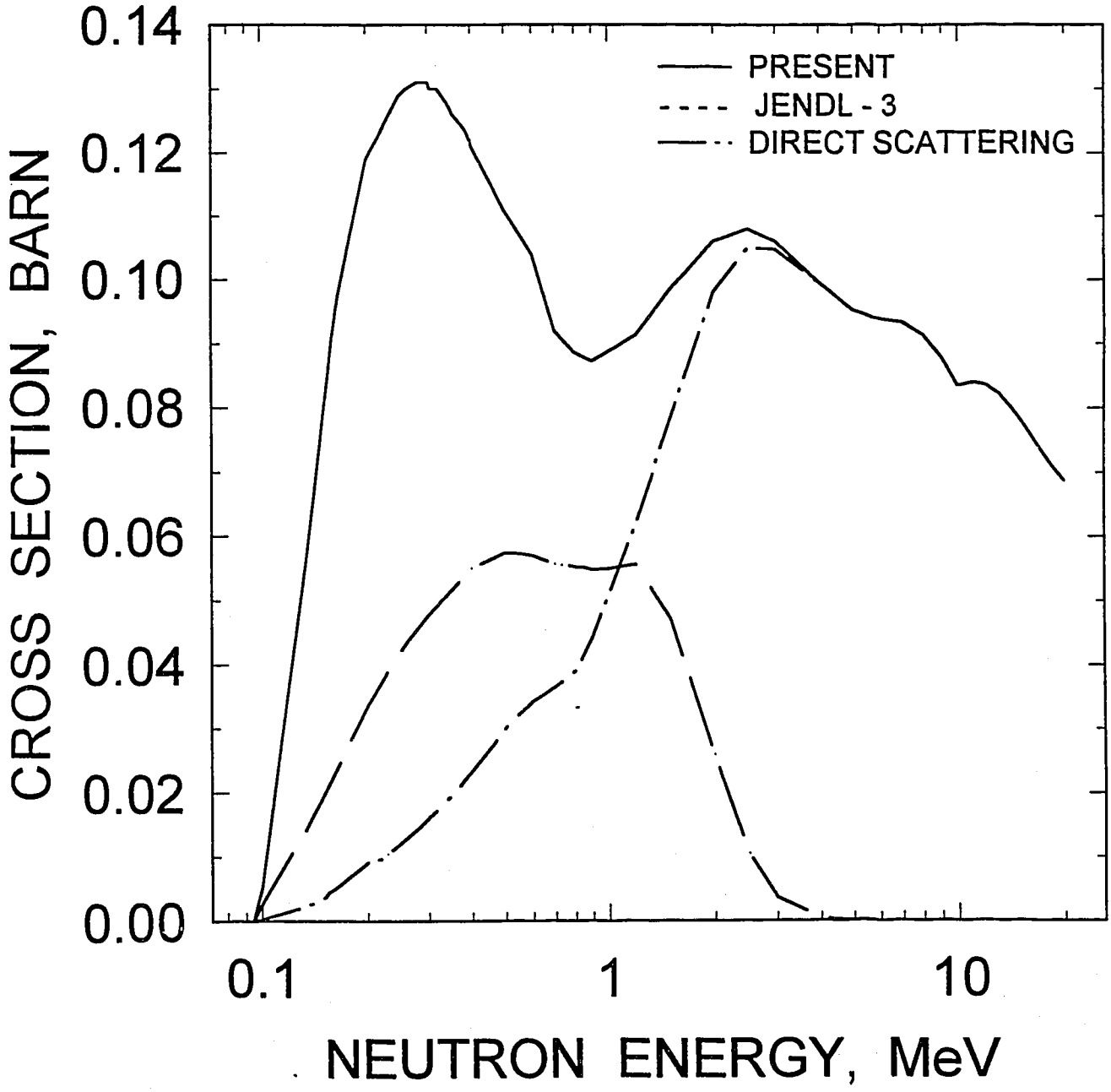

FIG. 4.10

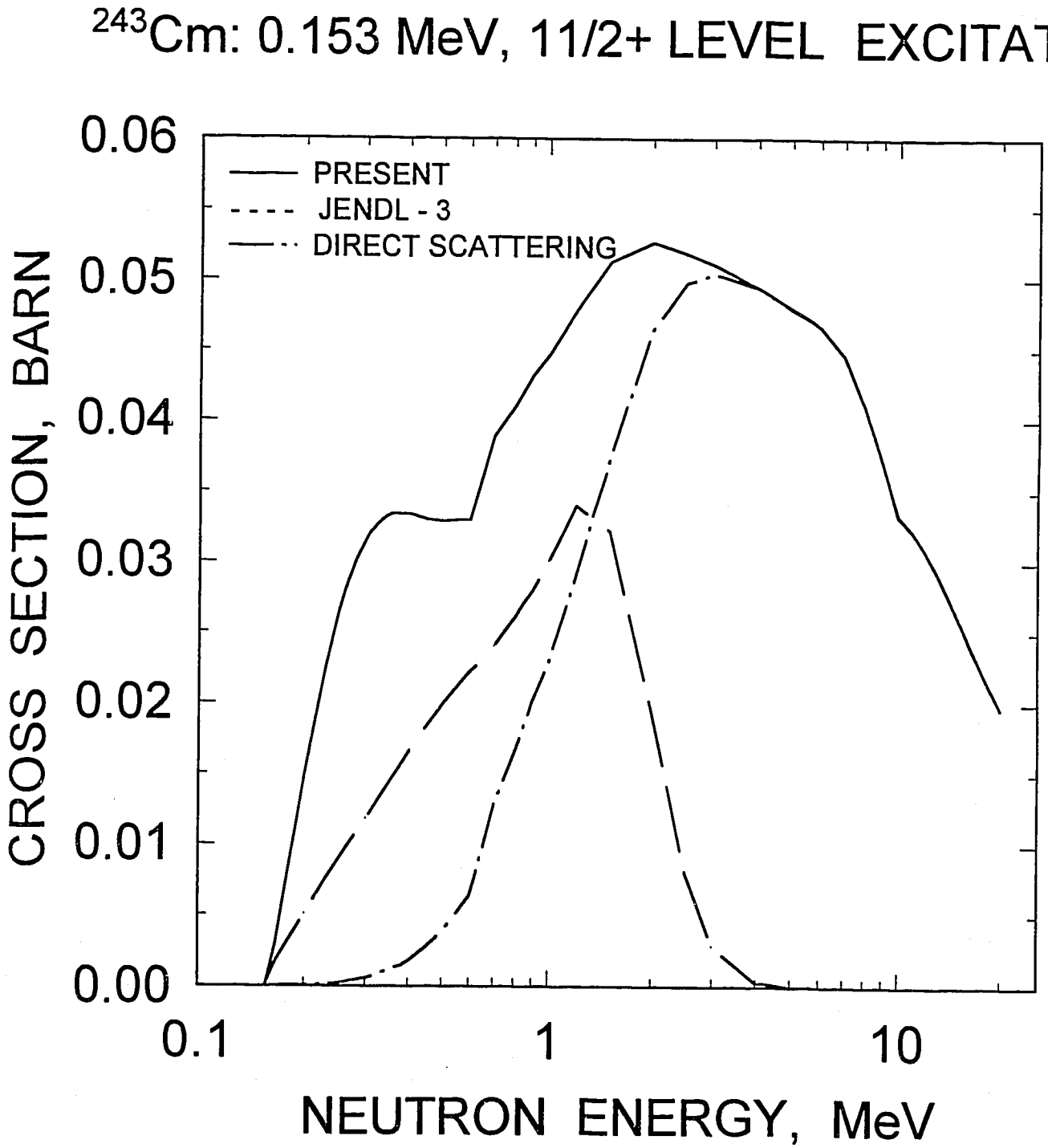
^{243}Cm: 0.153 MeV, 11/2+ LEVEL EXCITATION
PRESENT
JENDL - 3
DIRECT SCATTERING
CROSS SECTION, BARN
0.06
0.05
0.04
0.03
0.02
0.01
0.00
0.1
1
10
NEUTRON ENERGY, MeV

FIG. 4.11

^{243}Cm: 0.219 MeV, 13/2+ LEVEL EXCITATION

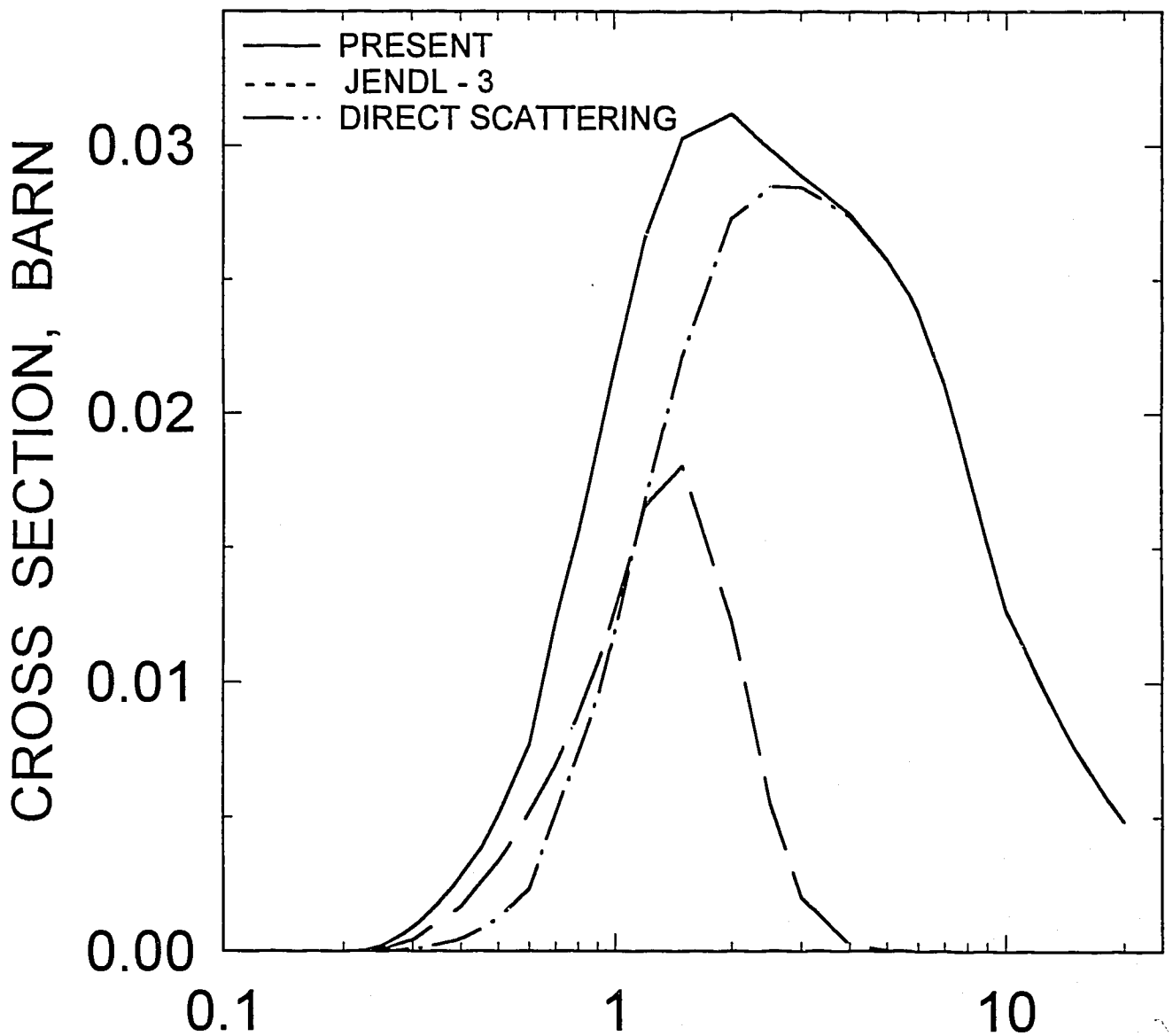

FIG. 4.12

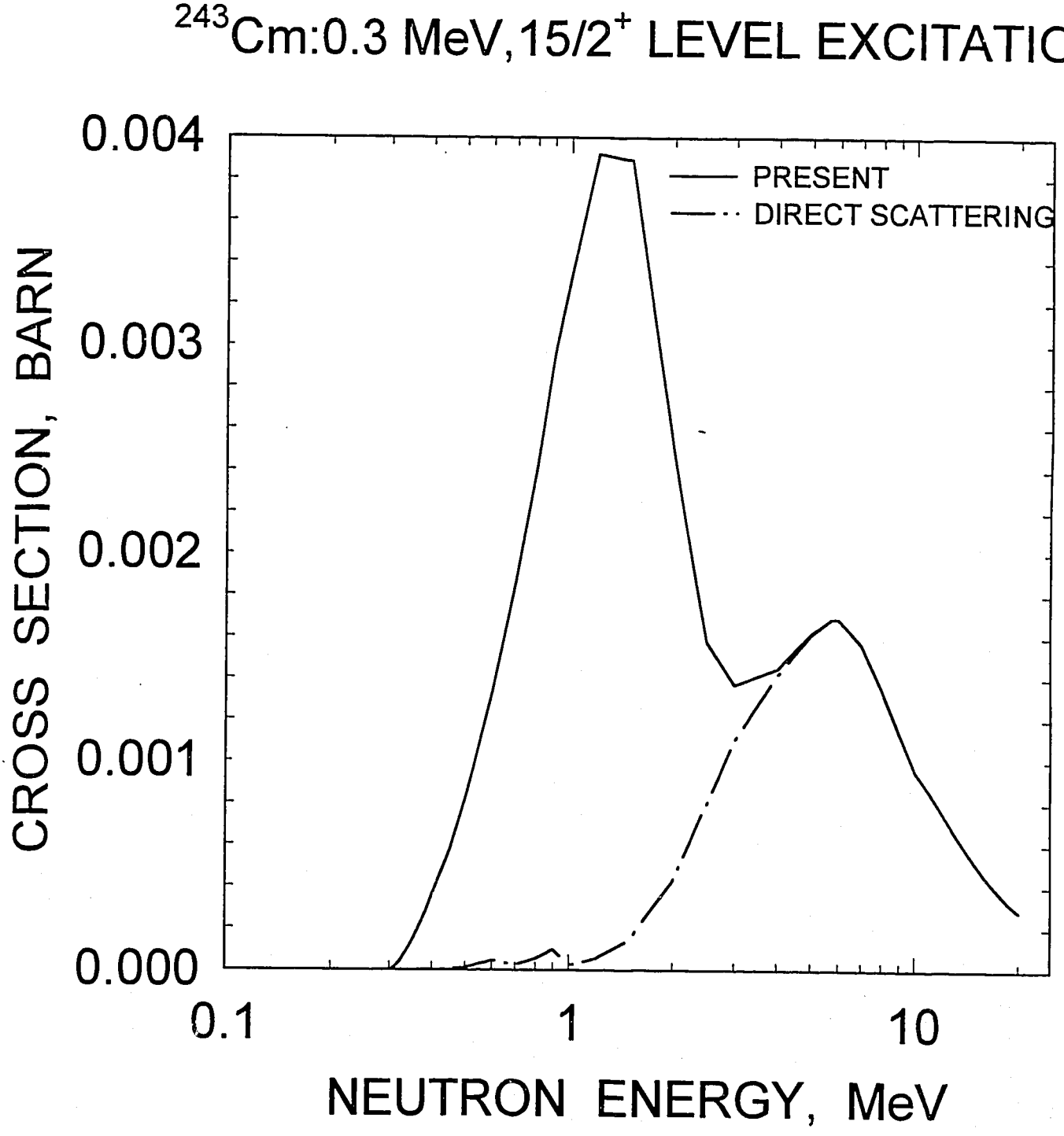
^{243}Cm:0.3 MeV,15/2^{+} LEVEL EXCITATION
PRESENT
DIRECT SCATTERING
CROSS SECTION, BARN
0.004
0.003
0.002
0.001
0.000
0.1
1
10
NEUTRON ENERGY, MeV

FIG. 4.13

^{243}Cm (n,γ) RADIATIVE CAPTURE CROSS SECTION

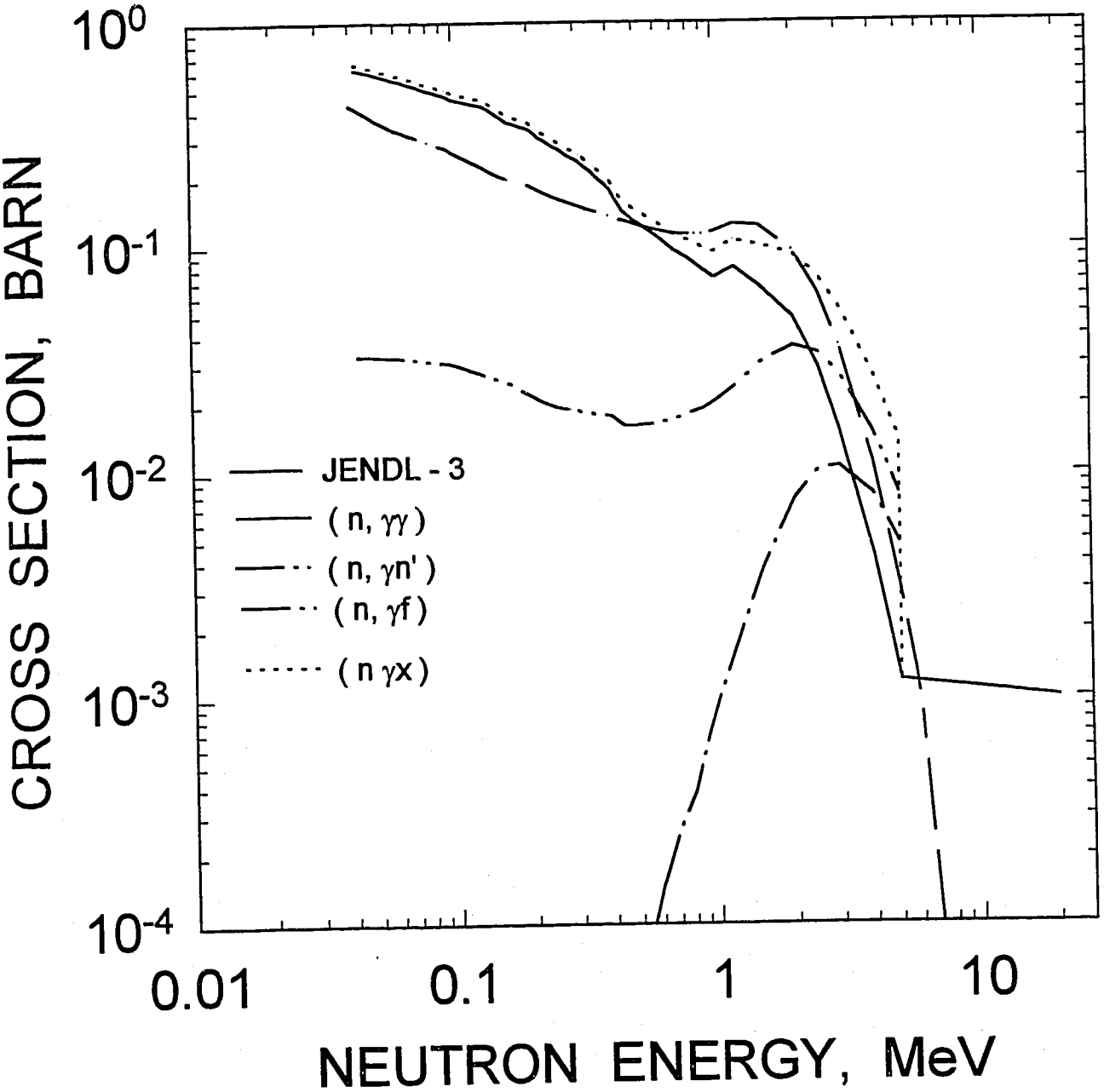

FIG. 4.14

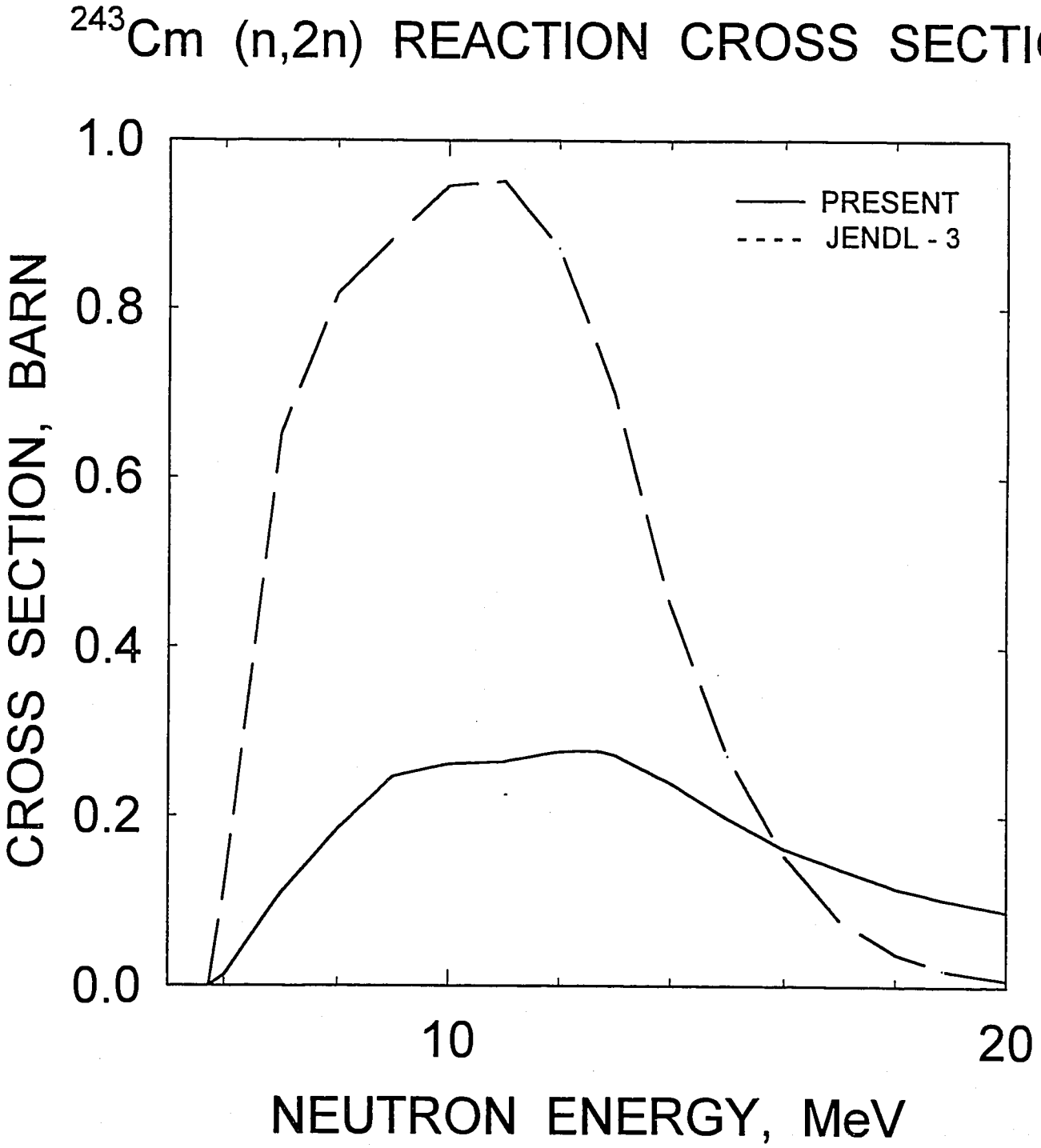
^{243}Cm (n,2n) REACTION CROSS SECTION
1.0
0.8
0.6
0.4
0.2
0.0
CROSS SECTION, BARN
PRESENT
JENDL - 3
10
20
NEUTRON ENERGY, MeV

FIG. 4.15

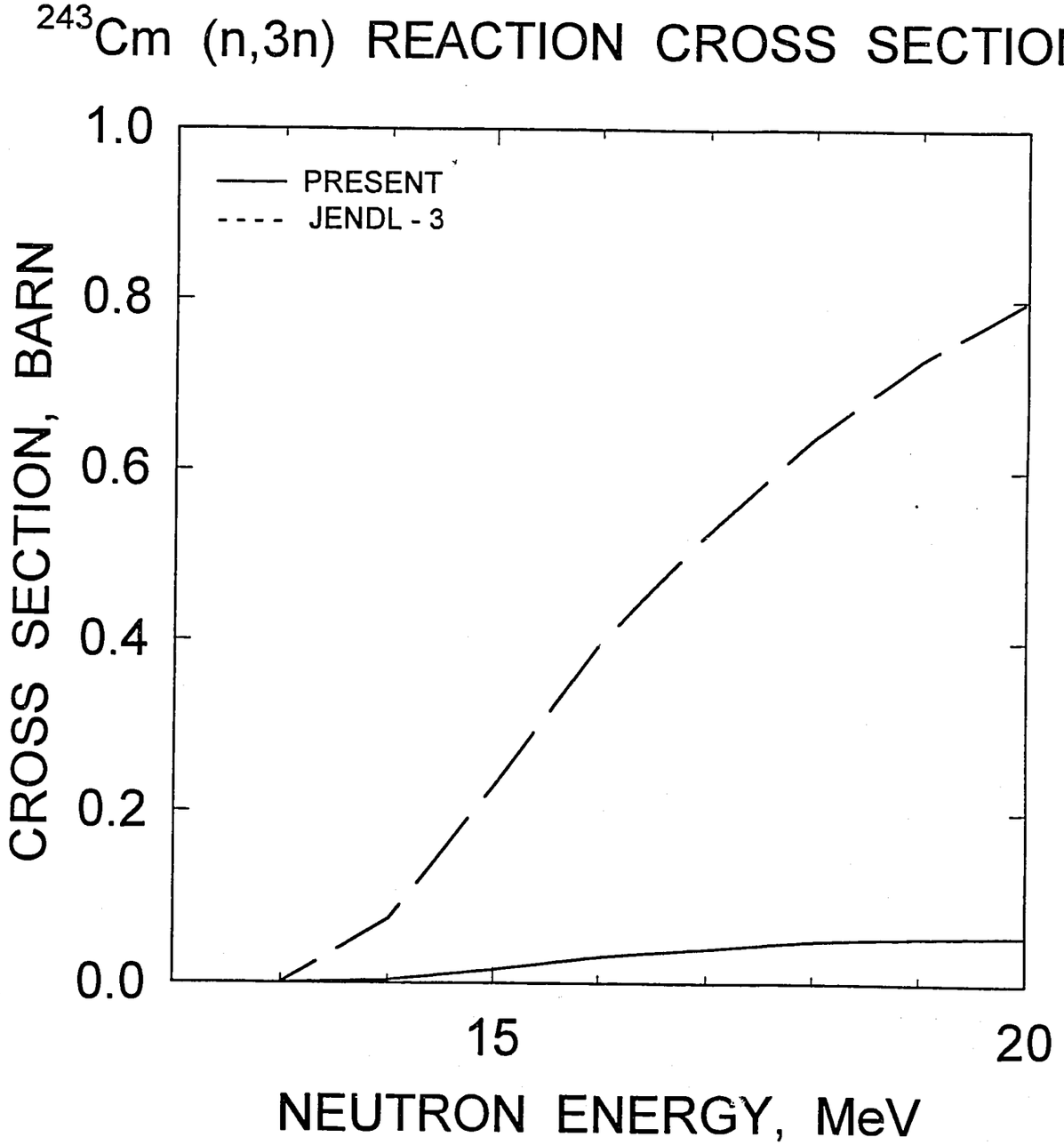
^{243}Cm (n,3n) REACTION CROSS SECTION
PRESENT
JENDL - 3
CROSS SECTION, BARN
1.0
0.8
0.6
0.4
0.2
0.0
15
20
NEUTRON ENERGY, MeV

FIG. 4.16

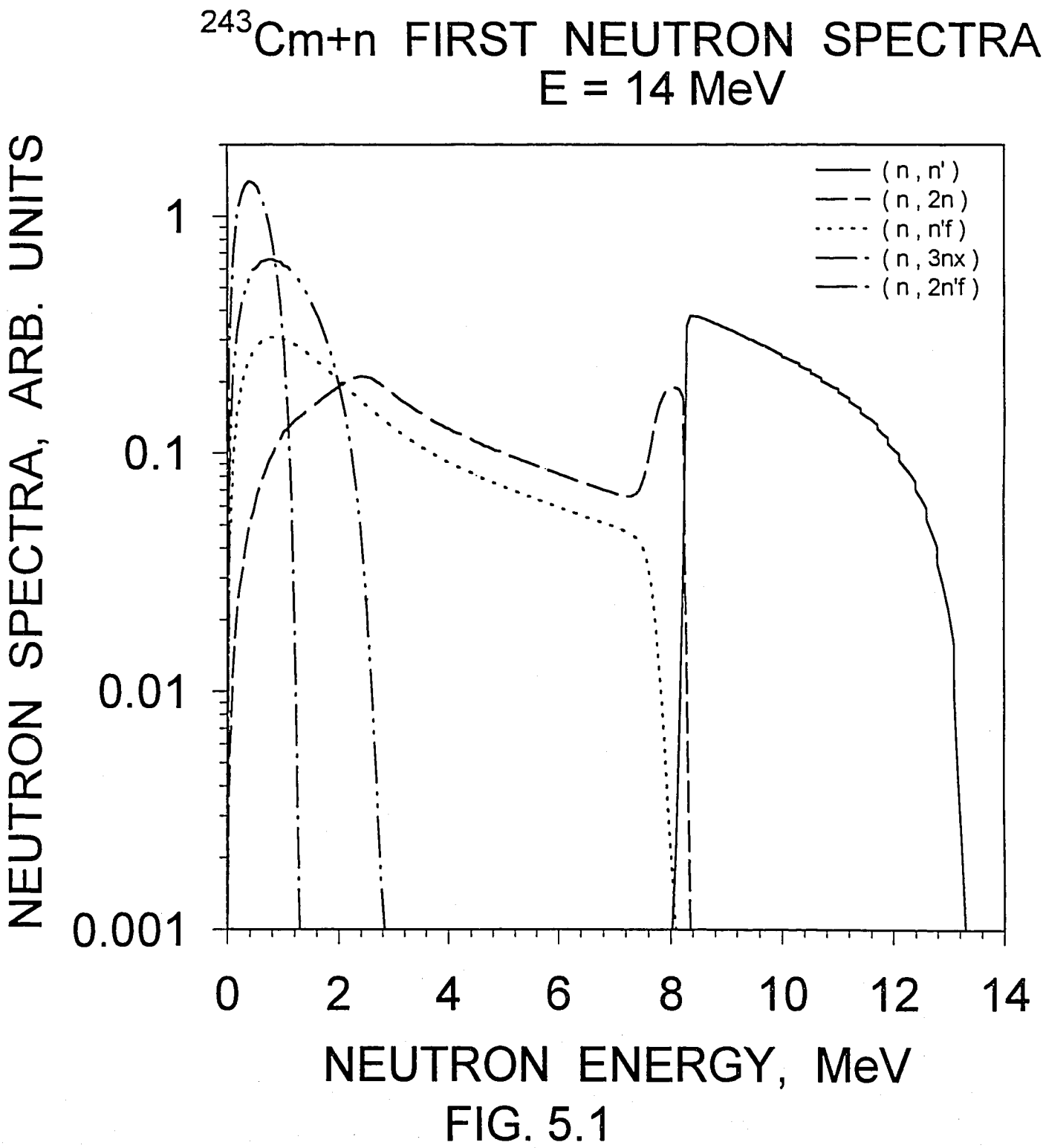
^{243}Cm+n FIRST NEUTRON SPECTRA
E = 14 MeV
NEUTRON SPECTRA, ARB. UNITS
1
0.1
0.01
0.001
0
2
4
6
8
10
12
14
NEUTRON ENERGY, MeV
(n , n')
(n , 2n)
(n , n'f)
(n , 3nx)
(n , 2n'f)

FIG. 5.1

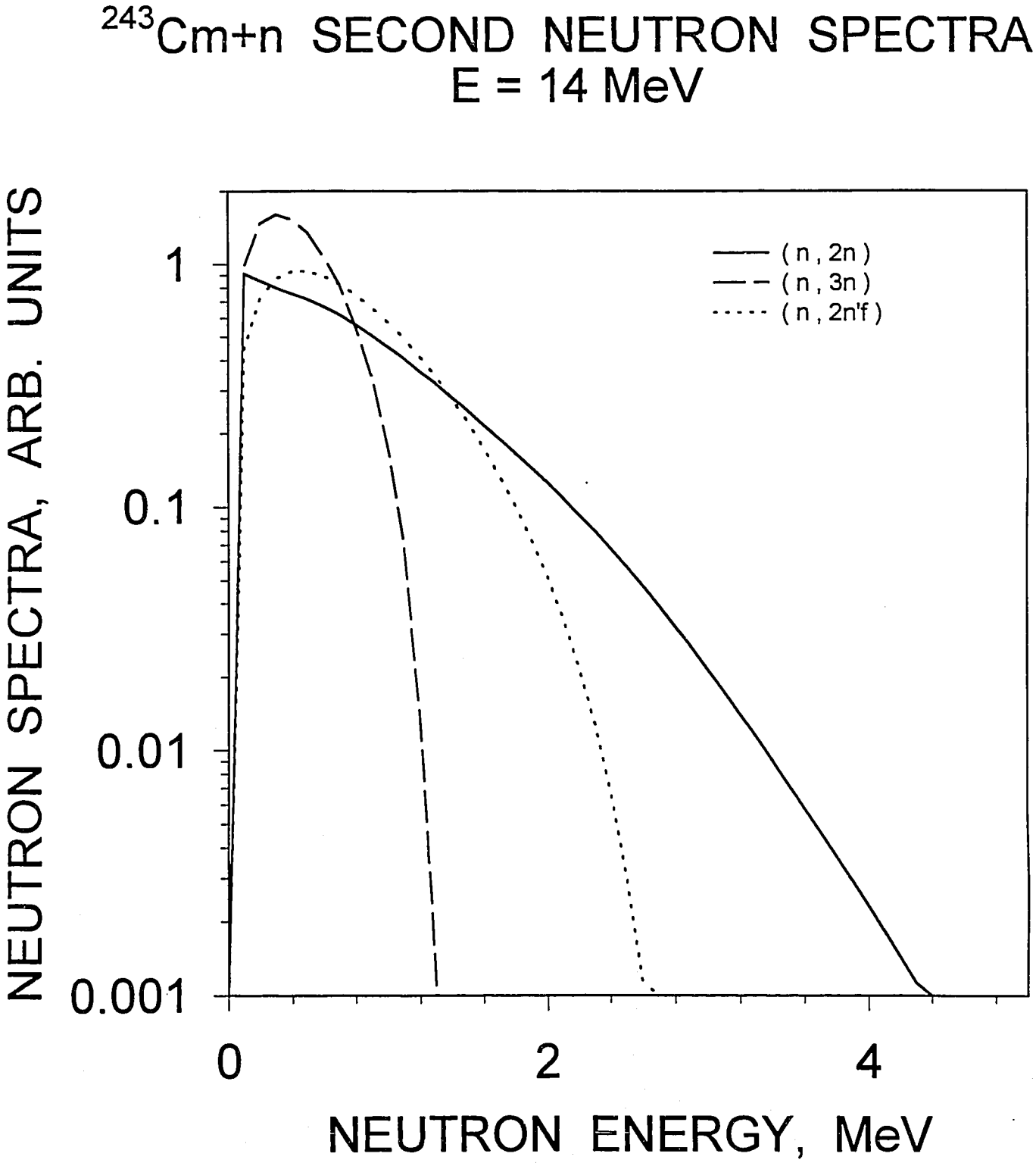
^{243}Cm+n SECOND NEUTRON SPECTRA
E = 14 MeV
NEUTRON SPECTRA, ARB. UNITS
1
0.1
0.01
0.001
0
2
4
NEUTRON ENERGY, MeV
(n , 2n)
(n , 3n)
(n , 2n'f)

FIG. 5.2

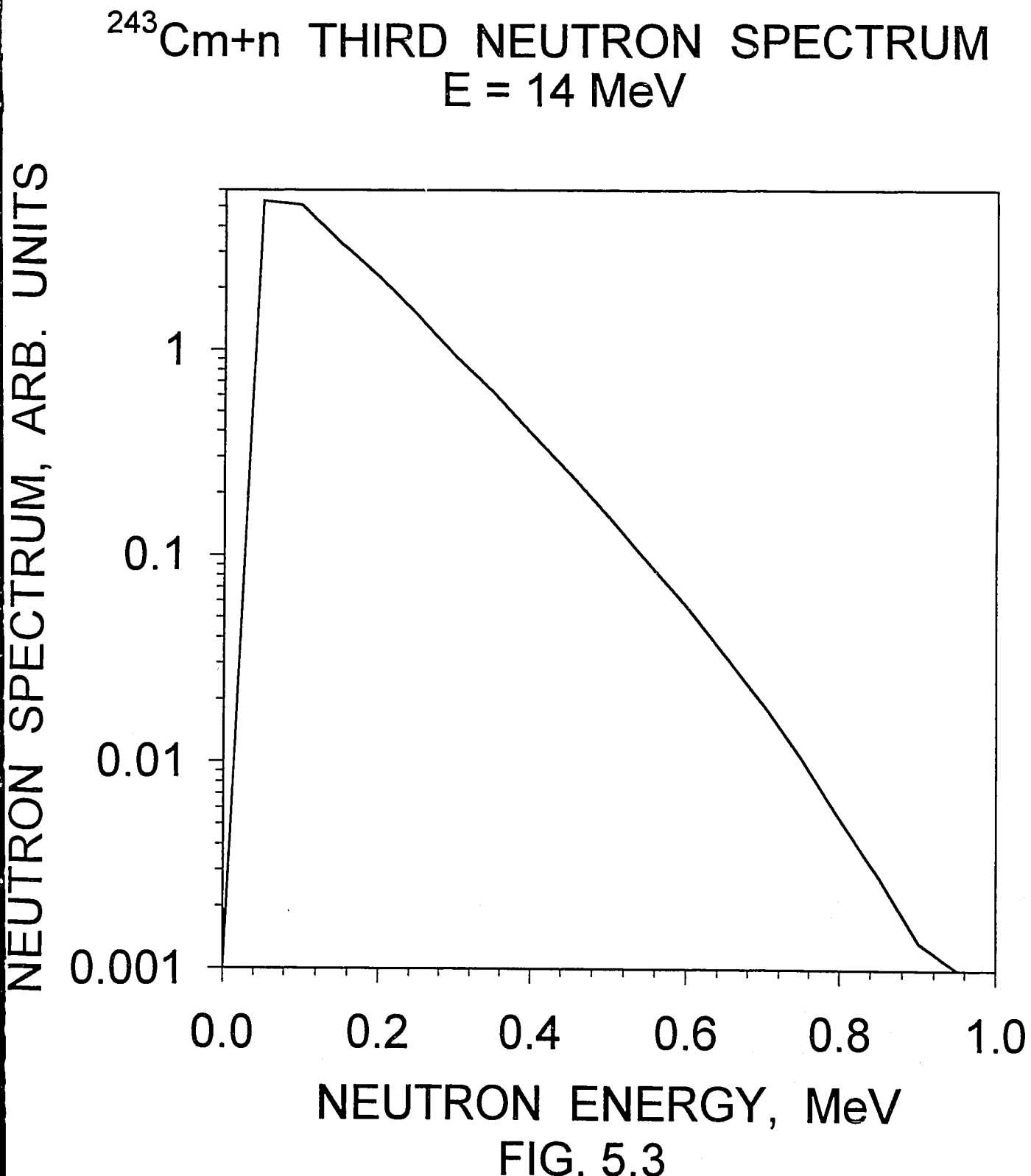
^{243}Cm+n THIRD NEUTRON SPECTRUM
E = 14 MeV
NEUTRON SPECTRUM, ARB. UNITS
1
0.1
0.01
0.001
0.0
0.2
0.4
0.6
0.8
1.0
NEUTRON ENERGY, MeV

FIG. 5.3

^{243}Cm PROMPT FISSION NEUTRON SPECTRU
RATIO TO MAXWELLIAN (T = 1.408 MeV

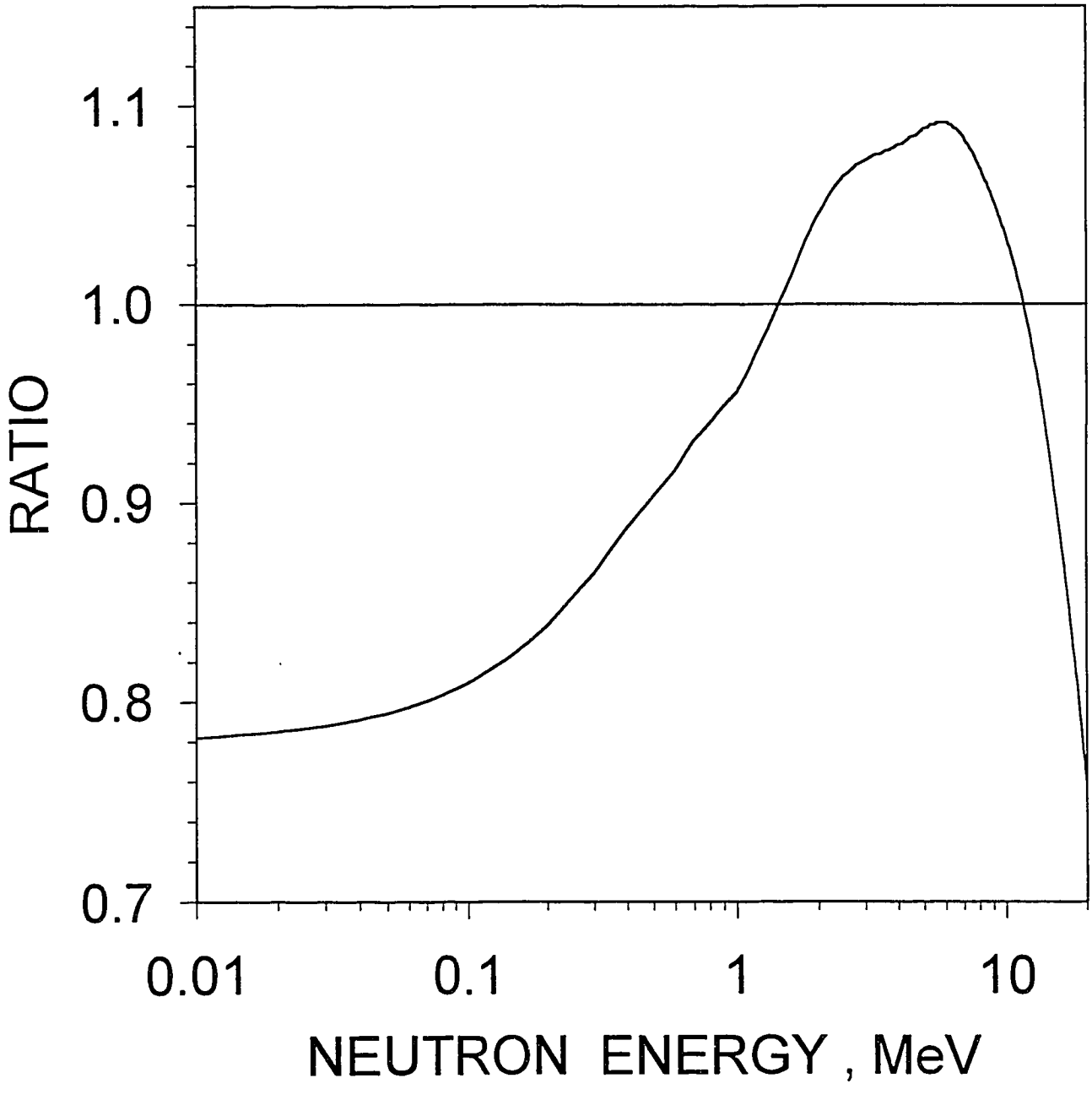

FIG. 5.4

^{243}Cm THERMAL PROMPT FISSION NEUTRON SPECTRUM

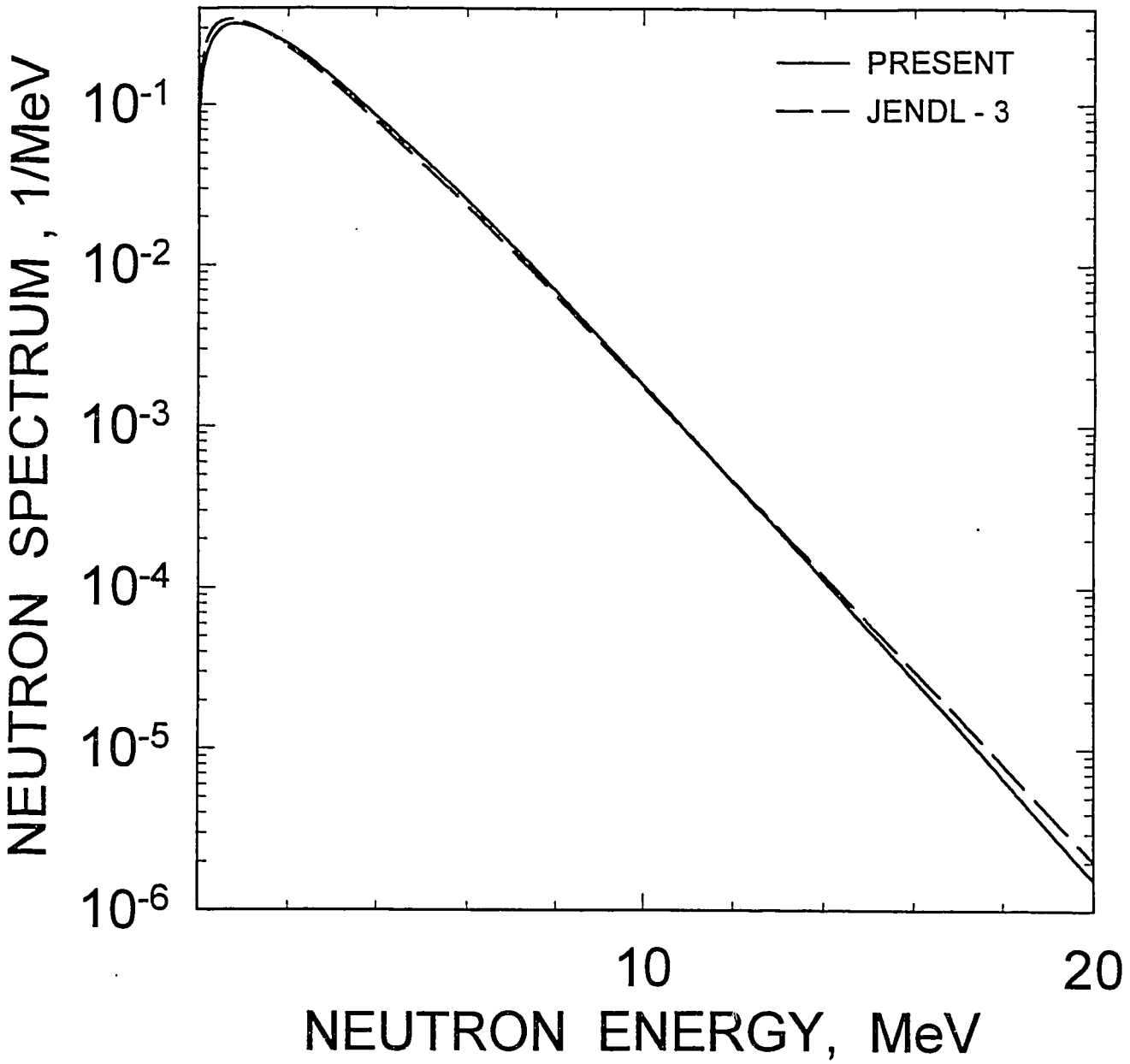

FIG. 5.5

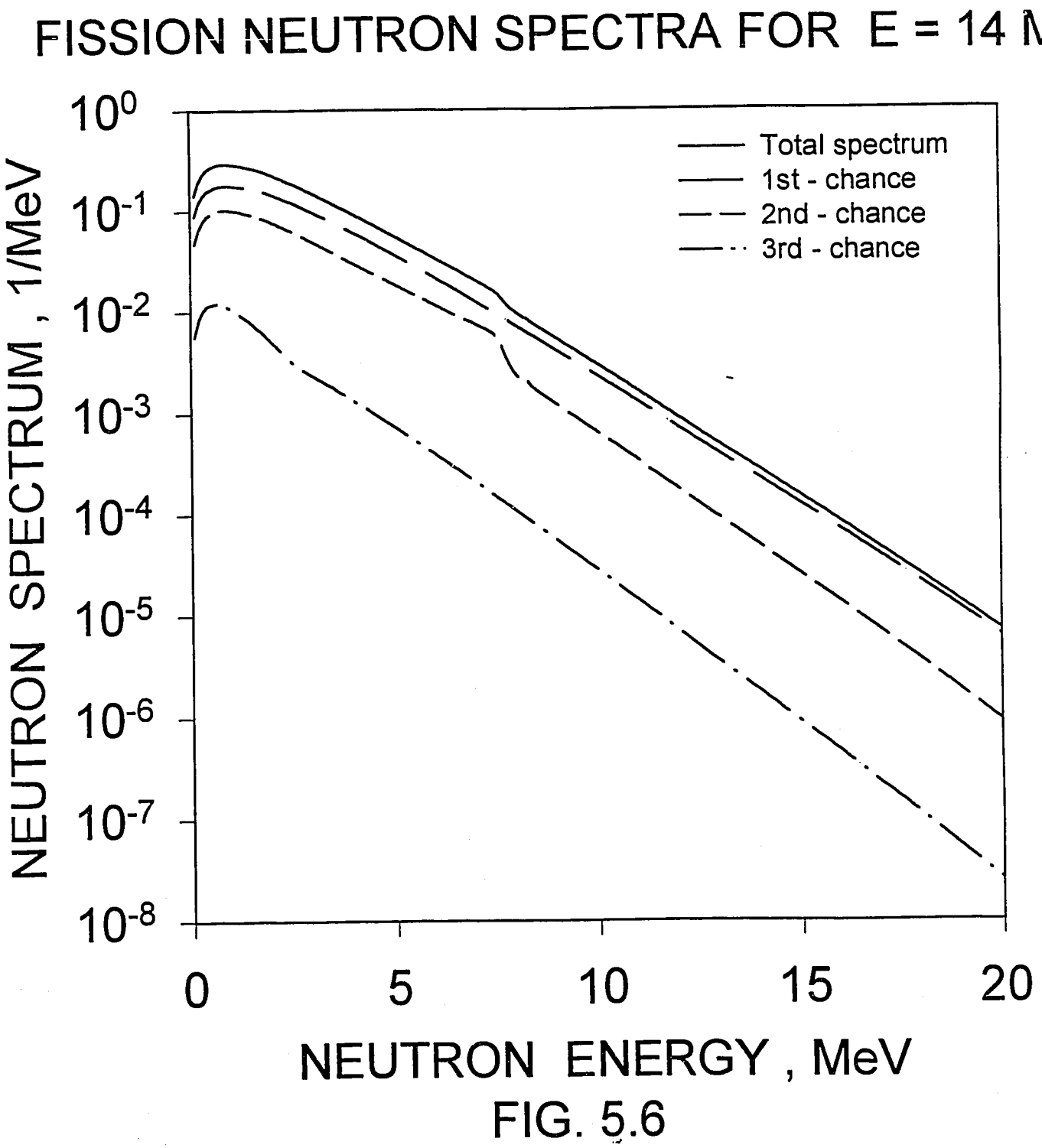
FISSION NEUTRON SPECTRA FOR E = 14 MeV
NEUTRON SPECTRUM , 1/MeV
10^{0}
10^{-1}
10^{-2}
10^{-3}
10^{-4}
10^{-5}
10^{-6}
10^{-7}
10^{-8}
Total spectrum
1st - chance
2nd - chance
3rd - chance
0
5
10
15
20
NEUTRON ENERGY , MeV

FIG. 5.6

^{243}Cm PROMPT FISSION NEUTRON MULTIPLICITY

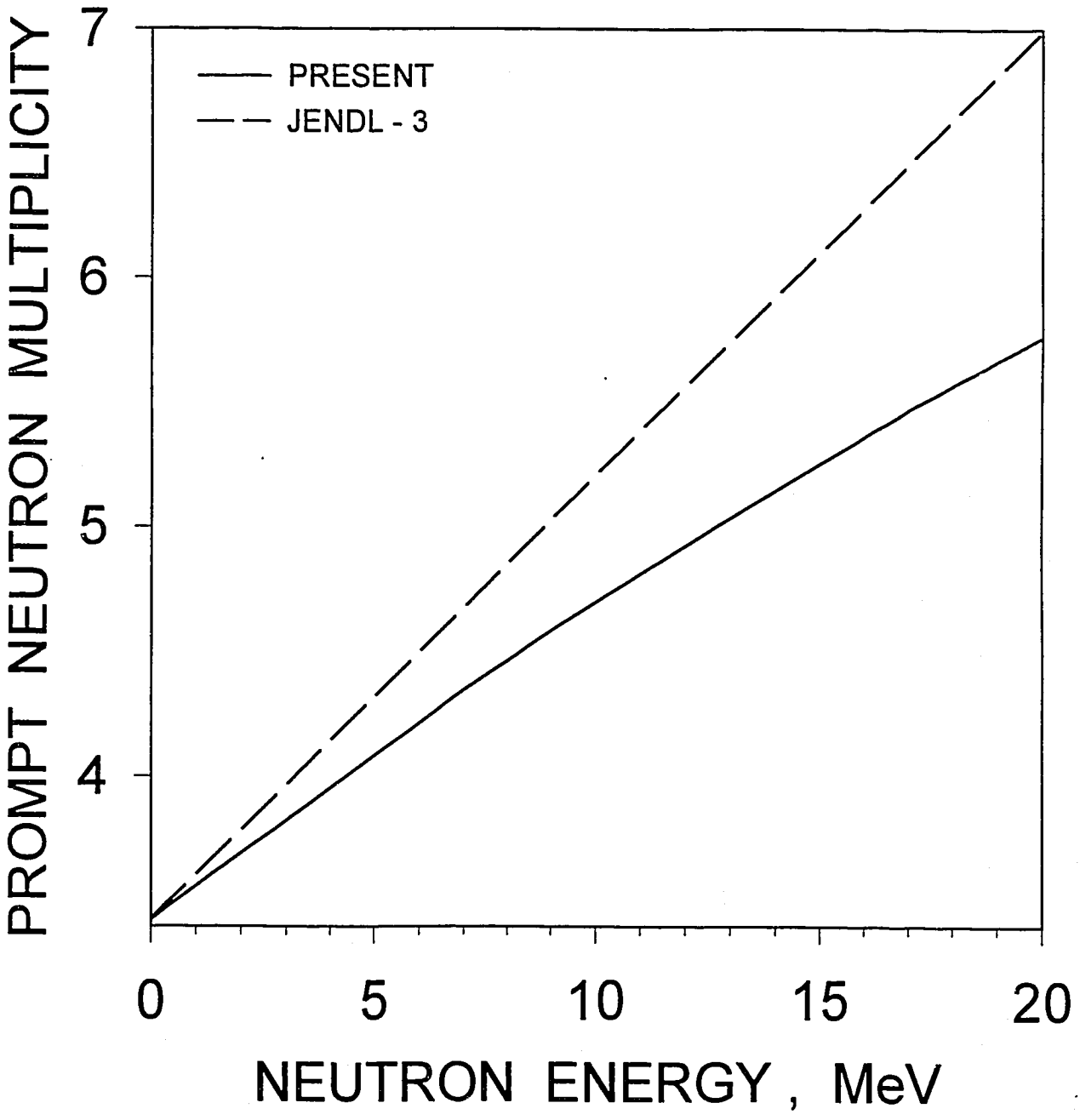

FIG. 6.1

Nuclear Data Section
International Atomic Energy Agency
P.O. Box 100
A-1400 Vienna
Austria

e-mail, INTERNET: SERVICES@IAEAND.IAEA.OR.AT
e-mail, BITNET: RNDS@IAEA1
fax: (43-1) 20607
cable: INATOM VIENNA
telex: 1-12645 atom a
telephone: (43-1) 2060-21710

online: TELNET or FTP: IAEAND.IAEA.OR.AT
username: IAEANDS for interactive Nuclear Data Information System
username: NDSOPEN for FTP file transfer